

**OF
THE
S
D**

**A Microstructure Dependant
Reactive Flow Model for
Heterogeneous Energetic Materials**

C.J. Doolan

DSTO-TR-1383

DISTRIBUTION STATEMENT A
Approved for Public Release
Distribution Unlimited

Best Available Copy

20030609 046



A Microstructure Dependent Reactive Flow Model for Heterogeneous Energetic Materials

C. J. Doolan

Weapons Systems Division
Systems Sciences Laboratory

DSTO-TR-1383

ABSTRACT

A new reactive flow model for heterogeneous energetic materials has been developed based on the physical and chemical parameters of the material as much as possible, rather than solely relying on empirical constants to determine the reaction rates behind the shock wave. Firstly, this report presents an extended viscoplastic pore collapse (hot spot) model based on previous models presented in the literature. Results from this hot spot model are then used to develop a reactive flow model embedded into the multi-material hydrocode, MULTI, using an Induction-Parameter-Model to describe the thermomechanical processes of pore collapse in a computationally efficient manner. One and two-dimensional hydrocode results are presented for the energetic material HMX undergoing bare and cased projectile impact. The results show the importance of microstructure in determining the shock ignition and subsequent growth behaviour in energetic materials. Thus, a new capability is described for determining the effects of varying porosity (due to manufacture, aging, damage, etc) on shock sensitivity and can be used to help evaluate the Insensitive Munitions (IM) qualities of weapon systems.

APPROVED FOR PUBLIC RELEASE

AQ F03-08-1883

DSTO-TR-1383

Published by

DSTO Systems Sciences Laboratory

PO Box 1500

Edinburgh, South Australia, Australia 5111

Telephone: (08) 8259 5555

Facsimile: (08) 8259 6567

© Commonwealth of Australia 2003

AR 012-547

February, 2003

APPROVED FOR PUBLIC RELEASE

A Microstructure Dependent Reactive Flow Model for Heterogeneous Energetic Materials

EXECUTIVE SUMMARY

A reactive flow model for porous energetic materials has been developed using a viscoplastic pore collapse model to describe hot spot generation, ignition and subsequent burning through a pressure dependent burn model. The viscoplastic pore collapse model is an extension of models from the literature and includes an enhanced combustion model with a BKW equation of state for the gases trapped within the pore. Results for HMX indicate that, after an initial thermal explosion within the pore, a quasi-steady state burning process occurs approximately at the shock pressure. These results were used to build a reactive flow model into a Eulerian multi-material hydrocode. Instead of imbedding the entire viscoplastic pore collapse model into the hydrocode, a computationally efficient Induction-Parameter-Model was developed. A shock initiation experiment for HMX was simulated using a one-dimensional model and it was found that a tri-modal initial pore distribution was required to obtain reasonable agreement. These results are also in agreement with another reactive flow model from the literature that solves the viscoplastic pore collapse equations at every time step. A two-dimensional simulation of a single fragment impact experiment was also performed. These results illustrate the importance of the interaction between the microstructure, material properties, wave structure, casing and fragment impact geometry. Hence, Weapons Systems Division now has a new modelling capability, enabling shock sensitivity calculations for energetic materials with varying amounts of porosity. The computationally efficient approach used here lends itself well to multi-dimensional simulations and can hopefully be used for Insensitive Munitions (IM) evaluations of future and in-service weapon systems.

Author

Con Doolan

Weapons Systems Division

Dr Con Doolan graduated from the University of Queensland in 1992 with a Bachelor of Mechanical Engineering. He later conducted research on hypervelocity wind tunnels and was awarded a Doctor of Philosophy from in 1997. Dr Doolan joined DSTO in 2000 after working at the University of Glasgow on helicopter aerodynamics. He now performs research on missile propulsion systems for the ADF and has interests in modelling shock ignition, cookoff response and advanced propulsion systems.

DSTO-TR-1383

Contents

1	Introduction	1
1.1	Shock Initiation of Energetic Materials	1
1.2	Hot Spot Mechanisms	2
1.3	Empirical Reactive Flow Models	3
1.4	Mechanistic Reactive Flow Models	4
2	Viscoplastic Pore Collapse Model	5
2.1	Model Description	5
2.2	Results	10
3	Reactive Flow Model	13
3.1	Model Description	13
3.2	One-Dimensional Results	21
3.3	Two-Dimensional Results	24
4	Summary, Conclusions and Future Work	26
5	References	27

Figures

1	A schematic illustrating the processes occurring during shock initiation in heterogeneous energetic material. The diagram shows an idealised projectile driving a shock wave through an energetic material sample.	2
2	Illustration of a cross section through an idealised spherical pore. Figure based on Kang et al. (1992).	6
3	Viscoplastic pore collapse results for HMX - internal pore radius and gas pressure history. $P_s = 2.2$ GPa, $\phi = 0.5\%$ and $a_o = 2.0 \mu\text{m}$	12
4	Viscoplastic pore collapse results for HMX - interface and gas temperature history. $P_s = 2.2$ GPa, $\phi = 0.5\%$ and $a_o = 2.0 \mu\text{m}$	12
5	Viscoplastic pore collapse results for HMX - reaction history. $P_s = 2.2$ GPa, $\phi = 0.5\%$ and $a_o = 2.0 \mu\text{m}$	13
6	Comparison of pore collapse gas pressure results for HMX. $P_s = 2.2$ GPa, $\phi = 0.5$ 3% and $a_o = 2.0 \mu\text{m}$	13
7	Comparison of pore collapse internal radius results for HMX. $P_s = 2.2$ GPa, $\phi = 0.5$ 3% and $a_o = 2.0 \mu\text{m}$	14
8	Comparison of pore collapse gas temperature results for HMX. $P_s = 2.2$ GPa, $\phi = 0.5$ 3% and $a_o = 2.0 \mu\text{m}$	14
9	Comparison of pore collapse HMX mass fraction results. $P_s = 2.2$ GPa, $\phi = 0.5$ 3% and $a_o = 2.0 \mu\text{m}$	15
10	Comparison of pore collapse nitrogen mass fraction results. $P_s = 2.2$ GPa, $\phi = 0.5$ 3% and $a_o = 2.0 \mu\text{m}$	15
11	Comparison of pore collapse gas pressure results for HMX. $P_s = 2.2$ GPa, $\phi = 1.5\%$ and $a_o = 0.5$ 2.0 μm	16
12	Comparison of pore collapse internal radius results for HMX. $P_s = 2.2$ GPa, $\phi = 1.5\%$ and $a_o = 0.5$ 2.0 μm	16
13	Comparison of pore collapse gas temperature results for HMX. $P_s = 2.2$ GPa, $\phi = 1.5\%$ and $a_o = 0.5$ 2.0 μm	17
14	Comparison of pore collapse HMX mass fraction results. $P_s = 2.2$ GPa, $\phi = 1.5\%$ and $a_o = 0.5$ 2.0 μm	17
15	Comparison of pore collapse nitrogen mass fraction results. $P_s = 2.2$ GPa, $\phi = 1.5\%$ and $a_o = 0.5$ 2.0 μm	18
16	Induction time (τ) versus Shock Pressure for HMX, $\phi = 0.5$ 3.0% and $a_o = 0.5$ 2.0 μm . Error bars indicate one standard deviation in computed results. Red line is a power law curve fit.	19
17	Go/no-go ignitability curve for HMX as calculated by the viscoplastic pore collapse model.	20
18	Schematic of one-dimensional numerical shock initiation model for HMX. . .	22

19	Numerical and experimental pressure records for HMX with 1.7% porosity. Dots represent experimental results while coloured lines indicate numerical results.	30
20	Space-time (x-t) diagram for one dimensional shock initiation simulation of HMX with 1.7% porosity. Contours are equally spaced values of pressure. . .	31
21	Comparison between numerical and experimental run to detonation distance for HMX with 1.7% porosity.	31
22	Numerical and experimental pressure records for HMX with varying porosity and a constant tri-modal pore distribution. Dots represent experimental results while coloured lines indicate numerical results.	32
23	Numerical and experimental pressure records for HMX with constant porosity and a varying tri-modal pore distribution. Dots represent experimental results while coloured lines indicate numerical results.	33
24	Schematic illustrating single fragment impact test.	34
25	Two-dimensional simulation of single fragment impact test. Results show coloured contours of pressure (top half of results) and equally spaced contours of fraction of reacted explosive (lower half).	35

DSTO-TR-1383

Tables

1	Stoichiometric coefficients for HMX reaction.	9
2	Parameters used for HMX in viscoplastic pore collapse model.	11
3	Equation of State Data used in one-dimensional numerical simulations.	22
4	Initial pore distributions for computational runs.	23

1 Introduction

This report documents a reactive flow model for energetic materials subjected to shock loading. In recent years shock initiation models have been developed which are relying less on empirical data to calibrate the model and more on the physical and chemical properties of the material. By developing such models shock sensitivity can be determined without a lengthy experimental program to calibrate the model and the effect of changes in microstructure can be determined computationally. For example, the effect of damage (increase in porosity) or change in particle size can be determined more quickly and inexpensively than by using a purely experimental approach.

It is of great advantage to those involved in the insensitive munitions community to be able to predict the high speed impact (shock) response of munitions with varying degrees of porosity or damage. Hydrocodes are the computational tool most commonly used to model shock initiation in energetic materials and the ignition process and subsequent chemical kinetics are described using a reactive flow model imbedded within the hydrocode. At present, the most reliable reactive flow models available are empirical and the most common and successful is the Lee and Tarver (1980) Ignition and Growth model. In order to use this model, an extensive series of experiments are required in order to determine empirical constants for the model. In the case of trying to determine the effect of increased porosity or damage, an expanded series of experiments are required for each microstructure which potentially could be very expensive and time consuming.

1.1 Shock Initiation of Energetic Materials

When a shock wave passes through an energetic material, it can respond in different ways depending on the intensity of the wave. If the wave is relatively weak, the energy transferred to the material is too small to initiate reaction and no response is recorded other than mechanical damage. If the wave strength is increased to a moderate level, chemical reactions are initiated but are quenched due to insufficient initial energy or from release waves from the sample/projectile boundaries, which quickly drop the pressure and temperature of the reaction zone. Increasing the wave strength beyond a shock initiation threshold value results in the shock-to-detonation transition (SDT). In this case the energy contained within the wave is sufficient to support sustained chemical reactions in the compressed region. In time, the pressure builds and drives a detonation wave through the material.

When early researchers calculated the bulk temperature in the compressed zone during the SDT process, it was found that the temperature was insufficient to cause the reactions observed in the energetic material. It was concluded that energy was concentrated into localised zones of increased temperature known as 'hot spots'. The chemical reaction rates are increased at these locations and if the conditions are right will result in sustained reaction of the material. Bowden and Yoffe (1952) were the first to suggest the existence of these hot spots and subsequently there has been a large amount of effort spent investigating the SDT process culminating in a certain consensus of opinion on the processes occurring during shock initiation of heterogeneous energetic material. This modern view of shock initiation is summarised in Fig. 1 and can be classified into four stages. The first stage

is during the initial shock passage into the material where energy is localised into hot spots (hot spot generation). If the size, number and intensity of hot spots are sufficient and the shock pressure is maintained for a sufficiently long period, chemical reactions are sustained and burning occurs at the hot spot sites. This represents the second stage of the process (ignition). As the hot spots are at discrete locations within the material, burning initially occurs on internal surfaces with the reaction front moving outward representing stage three (internal burning). When a reasonable proportion of the material has been consumed (estimated at 24-25% by volume), the burning surface switches from internal burning to external burning (stage four, external burning). This occurs when either hot spots 'burn-through' and burning is established around each individual grain or the solid material becomes sufficiently weak and fractures under the increasing pressure into smaller burning pieces suspended in the product gases. In reality, a combination of these processes is likely to occur.

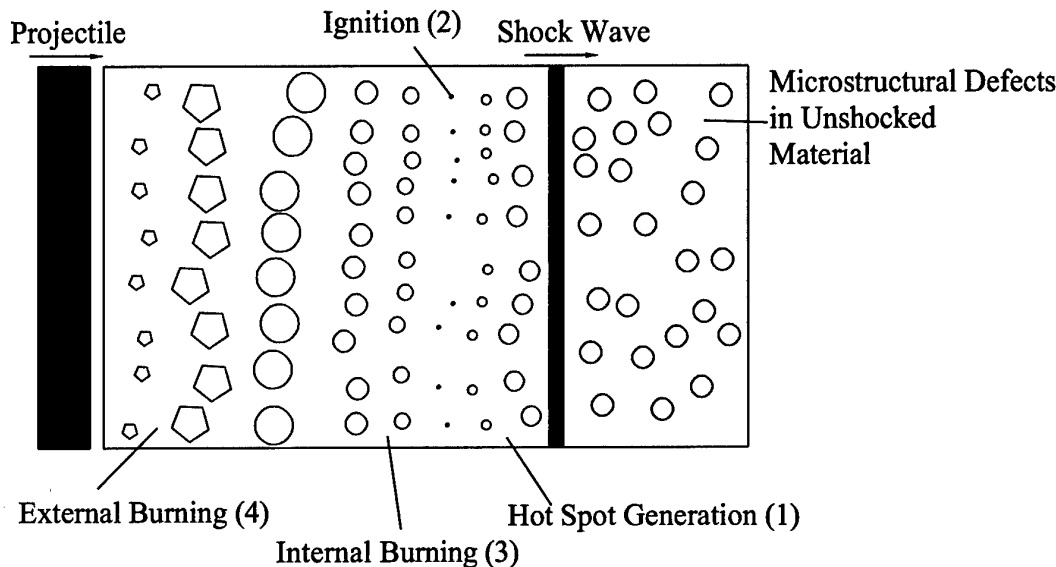


Figure 1: A schematic illustrating the processes occurring during shock initiation in heterogeneous energetic material. The diagram shows an idealised projectile driving a shock wave through an energetic material sample.

1.2 Hot Spot Mechanisms

There has been much debate and speculation over the physical mechanisms that cause hot spots during shock wave interaction with energetic materials. It is however, generally accepted that hot spots are caused by the interaction of a shock wave with defects in the microstructure of the energetic material and the formation process is controlled by the mechanical, thermodynamic and chemical properties of the material.

Many hot spot mechanisms have been proposed and despite the large amount of effort spent researching these phenomena, a single process has not been identified as the main energy localisation mechanism during shock initiation. A comprehensive list of hot spot

mechanisms will not be presented here however the reader is referred to Bonnet and Butler (1996) and Mellor et al. (1995) for a comprehensive list of possible mechanisms. Most hot spot mechanisms for shock initiation studies involve some kind of viscoplastic work and this is regarded as an efficient means of using shock energy to create high temperature localised zones.

The introduction of voids into an energetic material increases its shock sensitivity. This well known fact is used by explosive manufacturers to increase the detonability of their products. As mentioned previously, damaged energetic material also increases shock sensitivity as additional voids are introduced via the damage process. Therefore, it is suggested that shock induced void collapse is a likely hot spot generation mechanism for porous, heterogeneous and damaged energetic materials. Again, a number of void collapse models have been postulated. A successful technique that incorporates many physical processes is the viscoplastic pore collapse model. This technique is based upon the work of Carroll and Holt (1972) who investigated the interaction of shock waves and porous, ductile metal. Khasainov et al. (1981) extended this work to energetic materials as did Partom (1981), Frey (1984), Kang et al. (1992), Bonnet and Butler (1996) and Massoni et al. (1999).

The viscoplastic void collapse model assumes each void is a spherical, gas filled pore. When the shock passes over the pore, it begins to collapse. Heat generation is caused by the compression of the cavity gas and viscoplastic shearing in the highly stressed zone of material near the pore surface. Thermal conduction into the bulk of the material moderates the temperature. Material phase changes and chemical reactions are also taken into account to predict the onset of burning or explosion.

1.3 Empirical Reactive Flow Models

Hydrocodes commonly use empirical reactive flow models to determine the shock sensitivity of energetic materials. Probably the most widely used model is the Lee and Tarver (1980) Ignition and Growth model. This has been very successful in modelling the shock initiation of several explosives and propellants. It is usually expressed as a three term model (Tarver et al., 1996),

$$\frac{dF}{dt} = I(1 - F)^b \left(\frac{\rho}{\rho_0} - 1 - a \right)^x + G_1(1 - F)^c F^d P^y + G_2(1 - F)^e F^g P^z \quad (1)$$

where F is the fraction of energetic material reacted, t is the time, ρ is the material density, ρ_0 is the initial material density, P is the pressure and the remaining variables in Eq. 1 are empirical constants. The first term describes hot spot ignition by igniting some of the material relatively quickly but limiting it to a small proportion of the total solid (F_{igmax}). The second term represents the growth of reaction from the hot spot sites into the material and describes the inward and outward grain burning phenomena. This term is limited to a proportion of the total solid (F_{G1max}). The third term is used to describe the rapid transition to detonation observed in some energetic materials.

The Ignition and Growth model works well for single shock waves but must be used with care for multiple shock initiation (Tarver et al., 1995) and cannot predict the effects

of particle size or porosity without empirically classifying each material with differing grain size or porosity.

The forest fire reaction rate model (Mader, 1998) is also widely used. This model uses empirical 'pop-plots' or the run-to-detonation distance and single curve build up principle to describe the shock initiation process. Johnson, Tang and Forest (1985) incorporated some of the principles of the forest fire model into their JTF reactive flow model. This empirical model recognised that the temperature and distribution of hot spots was important and required an estimation of initial hot spot temperature and how it develops as a function of shock pressure.

The CPeX code (Jones and Kennedy, 1991) uses the reactive flow model of Kirby and Leiper (1985) to study the detonation processes in non-ideal explosives such as PBXW-115. This model accounts for hot spot ignition and subsequent burning through pre-determined stages defined by Gaussian functions. While successful, empirical data is required to describe the various stages of reaction in terms of time constants and mass fractions of various components.

Other empirical models are also available (e.g. Anderson et al., (1981), Partom and Wackerle (1989)) however they require specific information calibrated from experiments that do not easily allow for the adjustment of porosity or grain size.

1.4 Mechanistic Reactive Flow Models

Mechanistic reactive flow models attempt to incorporate the physics of hot spot formation with a burn model (kinetics) to describe shock initiation and detonation. The advantage of these models is that a more complete description of the shock initiation process can be gained thus enabling a deeper understanding of the physics occurring at the meso-scale. Hence, the user can investigate the effect of varying microstructural properties on shock sensitivity without resorting to empirical fits.

Unfortunately, modelling all the processes occurring within the energetic material is very computationally expensive. Baer et al., (1998) attempted this by using a high-resolution shock physics code to model mesoscale shock interactions in a random packed array of HMX crystals representing a small piece of explosive. Hot spot generation was shown to occur at the microstructural defects in the material due to shock focussing and plastic deformation. However, only a simple burn model was incorporated due to the high computational cost. To simulate a 1.2 mm x 0.9 mm x 0.9 mm sample at 68% theoretical maximum density (TMD) required the entire Sandia National Laboratories TFLOP (10^{12} floating point operations per second) computer using 4500 processors with 104 MB/processor. It is obvious that to use this method to model larger amounts of energetic material at higher TMD and with improved chemical kinetics will require significant advances in computational performance.

Similarly, Conley et al. (1998) perform microscale simulations of PBX-9501 using a 2D Eulerian hydrocode and a mesh derived directly from a micrograph of a PBX section. Important results were obtained on hot spot temperature and size, however a reactive flow model was not included presumably because of the high computational cost.

A less computationally demanding approach is to use a continuum based mechanistic reactive flow model imbedded into an existing hydrocode. In this type of model, the mechanisms of hot spot formation and subsequent burning are assumed in advance and applied throughout the energetic material. Recent examples of this type of mechanistic reactive flow model can be found in Cook et al. (1998) or Bennett (1998). Making appropriate assumptions about how the hot spots are formed, ignited and burnt can lead to a considerable reduction in the amounts of computational resources required. The disadvantage is that a single hot spot formation and ignition theory cannot be agreed upon, which may raise doubts about the validity of the model.

As mentioned previously, the viscoplastic pore collapse model of hot spot generation has been used with success by a number of researchers. Plastic deformation has also been identified as an efficient method of localising shock wave energy. Massoni et al., (1999) have developed a mechanistic reactive flow model based upon viscoplastic pore collapse. The model was used to successfully describe one-dimensional shock initiation in pressed HMX. Despite the assumptions used, this model is still rather computationally expensive, requiring approximately 150+ equations to be solved simultaneously. This effectively limits the model to one-dimensional problems using the current computer systems in Weapons Systems Division, DSTO. This report will outline a new reactive flow model based upon the work of Massoni et al., (1999) which is less computationally expensive and will allow two-dimensional simulations of shock initiation. This provides a useful simulation tool for those assessing weapons systems for unplanned stimuli.

2 Viscoplastic Pore Collapse Model

2.1 Model Description

The viscoplastic pore collapse model of Kang et al. (1992) has been used to describe the processes occurring during hot spot formation. This model has been modified and extended by Bonnett and Butler (1996) and later by Massoni et al. (1999). The model presented below represents another extension of the Kang et al. (1992) model. Here, a more detailed description of the heat release due to chemical reactions is used in conjunction with the BKW equations of state. The results of this model are used to develop the reactive flow model presented in the next section.

Figure 2 illustrates the mechanisms assumed during viscoplastic pore collapse. Following previous work, the porosity of the energetic material in question is matched in the micromechanical model by using the equation,

$$\phi = \left(\frac{a}{b}\right)^3, \quad (2)$$

where ϕ is the porosity and a, b are the inner and out radii respectively as described in Fig. 2. Hence the average pore size in the bulk of the energetic material is used to determine a while the bulk material porosity ϕ is used with Eq. 2 to determine b .

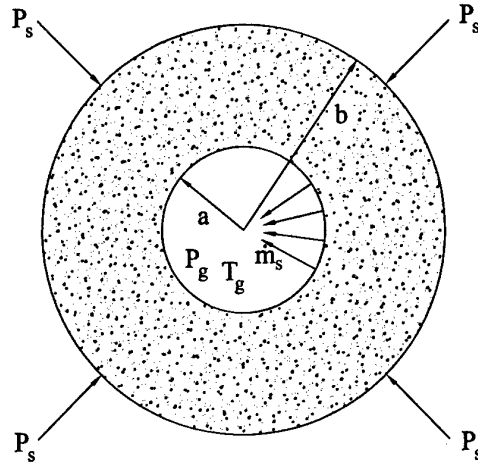


Figure 2: Illustration of a cross section through an idealised spherical pore. Figure based on Kang et al. (1992).

The shock is assumed to pass over the pore instantaneously, setting up a hydrostatic pressure field in the material surrounding the pore. This assumption is thought to be valid for small pore sizes up to a few tens of micrometres. For larger pore sizes, asymmetric collapse of the pore occurs, resulting in a complex flow pattern, sometimes with material jetting across the pore. Therefore this model is limited to pore sizes of a few tens of μm .

Shock pressures experienced by energetic materials during shock initiation are usually greater than 1 GPa. In this pressure range, the mechanical strength of the material is quickly overwhelmed and the pore collapses under the action of rapid viscoplastic flow. As the pore collapses, intense heating occurs near the pore surface under the combined action of plastic and viscous flow. Eventually, the temperature increases to a level where phase change occurs at the pore surface. There is some debate over whether the phase change involves melting at the surface with chemical reactions occurring in the condensed phases (Bonnett and Butler, 1996) or sublimation directly into the gas phase with the bulk of the energy release occurring in the gas phase (Kang et al., 1992, Massoni et al., 1999). Here we assume that sublimation occurs at the surface with all combustion occurring in the gas phase.

The motion of the pore surface is described by the following equation derived by Massoni et al. (1999),

$$\frac{d\xi}{dt} = \frac{1}{\rho_s a (1 - \phi^{\frac{1}{3}})} \left\{ P_g - P_s - 4\mu_s \frac{\xi}{a} (1 - \phi) \right. \\ \left. \dot{m}^2 \left(\frac{1}{\rho_s} - \frac{1}{\rho_g} \right) - 2\bar{Y}_s \text{sign}(\xi) \ln \left(\frac{a}{b} \right) \right. \\ \left. \frac{1}{2} \rho_s \xi \left[4 \left(\xi + \frac{\dot{m}}{\rho_s} \right) (1 - \phi^{\frac{1}{3}}) - \xi (1 - \phi^{\frac{4}{3}}) \right] \right\}, \quad (3)$$

where $\xi = \dot{a} - (\dot{m}/\rho_s)$, t is the time, \dot{m} is the mass flow rate at the pore surface, ρ_s is the density of the solid, P_g is the pressure of the pore gas, P_s is the shock pressure, μ_s is

the viscosity of the solid phase and \bar{Y}_s is the yield strength of the solid phase. Equation 3 is very useful as it applies the viscoplastic resistance with the gas pressure against the shock pressure to provide an equation of motion for the pore surface with a correction for mass flux due to sublimation.

The mass flux condition at the surface is defined by,

$$[\rho_s (\dot{a} - u_s)]_{r=a} = [\rho_g (\dot{a} - u_g)]_{r=a} = \dot{m}, \quad (4)$$

where u_s and u_g are the velocities of the solid and gas phases respectively.

The solid phase velocity is controlled through the following equation of motion,

$$u_s(r) = \left(\frac{a}{r}\right)^2 \xi. \quad (5)$$

Some of the heat generated from viscoplastic work and gas compression is conducted through the pore material. The transient temperature profile through the pore material is calculated by solving the unsteady one-dimensional spherical heat equation,

$$\rho_s c_s \frac{\partial T_s}{\partial t} = k_s \left(\frac{\partial^2 T_s}{\partial r^2} + \frac{2}{r} \frac{\partial T_s}{\partial r} \right) + \Phi_s, \quad (6)$$

where c_s is the specific heat of the solid phase, t is time, k_s is the conductivity of the solid phase, T_s is the temperature of the solid phase, r is the radial position and

$$\Phi_s = 12\mu_s \left(\frac{u_s}{r}\right)^2 + 2\bar{Y}_s \left(\frac{|u_s|}{r}\right), \quad (7)$$

is the viscoplastic heating source term. Equation 6 is solved at each time step using an implicit Gauss-Seidel numerical procedure with successive over-relaxation. An adiabatic boundary condition is applied to Eq. 6 for the outside of the pore material. For the inner surface, the boundary condition is set to,

$$k_g \left(\frac{\partial T_g}{\partial r} \right)_{r=a} = 5k_g \frac{T_i}{a} \frac{T_g}{a}, \quad (8)$$

where k_g is the conductivity of the gas phase, T_g is the pore gas temperature and T_i is the interface or inner pore surface temperature. Equation 8 was proposed by Massoni et al. (1999) who performed a systematic analysis to determine an approximation for the thermal profile across the pore and hence an estimate of the thermal boundary layer thickness. Once the inner surface starts to sublime, the inner boundary condition for Eq. 8 is set to zero.

The energy of the gas within the pore is increased by the compression imparted by the collapsing wall of the pore. It is also modified by the mass addition during sublimation and by chemical reaction. The specific total energy of the pore gas is given by,

$$E = e + \sum_{i=1}^{N_s} \frac{(\Delta H_f^o)_{T_R,i}}{M_i} f_i, \quad (9)$$

where E is the specific total gas energy, e is the specific internal energy, $(\Delta H_f^o)_{T_R,i}$ is the molar heat of formation of species i at the reference temperature $T_R = 0$ K, M_i is the molecular weight of species i , f_i is the mass fraction of species i and N_s is the total number of species in the gas mixture. The heat of formation term provides the mechanism for heat release and absorption during pore collapse.

The specific internal energy can be written as a function of temperature and the mass fraction of each of the individual species in the mixture,

$$e = \sum_{i=1}^{N_s} f_i e_i(T). \quad (10)$$

Following Sichel et al. (2002), the specific internal energy can be written in terms of the McBride and Gordon (1967) polynomials,

$$e = \sum_{i=1}^{N_s} R_i f_i \left\{ a_{6,j} + (a_{1,i} - \sigma) + \sum_{k=2}^5 \frac{a_{k,i}}{k} T^k \right\}, \quad (11)$$

where a_k are the polynomial constants (McBride and Gordon, 1967) and R_i is the gas constant for species i . Equation 11 has been modified to include the term σ from the BKW equation of state (described later in this report). This is done to include real gas effects that occur at the high shock pressures present during pore collapse.

Specific internal energy is modified by compression from the pore wall or from conduction into the energetic material. The rate of change of specific internal energy can be written as,

$$\dot{e} = \frac{3}{a\rho_g} \left(5k_g \frac{T_i}{a} \frac{T_g}{a} - P_g \dot{a} \right). \quad (12)$$

It is assumed that the conduction term (the first term in the brackets) is zero once sublimation begins.

Chemical reactions are assumed to occur in the gas phase only and to follow a single step, irreversible reaction involving twelve species (i.e. $N_s = 12$),

$$\alpha_1 Z_1 \rightarrow \sum_{i=2}^{N_s} \alpha_i Z_i, \quad (13)$$

where Z_i is the chemical symbol for species i and a_i is the stoichiometric coefficient for species i . In this report, calculations are performed using HMX energetic material. Table 1 lists the stoichiometric coefficients for the reaction used here. These were determined

Table 1: Stoichiometric coefficients for HMX reaction.

i	Z_i	α_i
1(Reactant)	HMX(gas)	1
2	O ₂	2.905e-5
3	N ₂	3.986
4	H ₂ O	3.472
5	CO ₂	0.564
6	CO	3.398
7	H ₂	0.412
8	NO	1.789e-3
9	NO ₂	3.729e-9
10	CH ₄	3.780e-2
11	CH ₃	3.802e-4
12	NH ₃	2.62e-2

by performing constant volume explosion simulations using the CHEETAH (Fried and Howard, 2001) software package.

The gas combustion is assumed to follow a single step Arrhenius law,

$$\dot{\omega} = f_1 A \exp \frac{E_a}{RT_g}, \quad (14)$$

where $\dot{\omega}$ is the rate of combustion of the reactant (HMX), A is the pre-exponential factor, E_a is the activation energy and R is the universal gas constant.

Sublimation is assumed to occur once the material reaches its melting temperature, which follows a linear relationship with shock pressure (Massoni et al., 1999),

$$T_m = T_{m0} + \beta P_s, \quad (15)$$

where T_m is the melting temperature, T_{m0} is the melting temperature at atmospheric pressure and b is a constant. Determining the sublimation rate is difficult as it represents the first step (pyrolysis) of the combustion process and hence is controlled by the kinetics of decomposition. As these rates are difficult to determine, a pressure-dependent sublimation law is assumed,

$$\dot{m} = \rho_s A_p a_v P_g^n, \quad (16)$$

where A_p is the pore surface area and a_v , n are constants. The assumption of sublimation occurring at the melt temperature has been chosen as a part of a convenient description of the combustion process first suggested by Massoni et al. (1999).

The specific internal energy is updated by determining the contributions from mechanical compression and conduction (Eq. 12) and changes in heat of formation. The temperature is calculated at each time step by solving Eq. 11 iteratively using a Newton-Raphson technique.

A Becker-Kistiakowsky-Wilson (BKW) equation of state is used to describe the state of the pore gas (Mader, 1998),

$$\sigma = \frac{P_g V_g}{RT_g} = 1 + X \exp \beta X, \quad (17)$$

where V_g is the molar gas volume and,

$$X = \frac{\kappa k}{V_g (T_g + \theta)^\alpha}, \quad (18)$$

where $\alpha, \beta, \theta, \kappa$ are parameters. Here we use the parameters given by Vauller and Espagnaq (1998) for nitramines. The value, k , is the average covolume,

$$k = \sum_{i=1}^{N_s} f_i k_i, \quad (19)$$

where, in this case, f_i represents the mole fraction of the gaseous species i and k_i is a constant covolume characteristic of species i . Equation 19 is summed over the gaseous species only.

2.2 Results

The viscoplastic pore collapse model has been used to investigate the physical processes occurring during shock ignition. Calculations were performed using cyclotetra-methylene-tetranitramine (HMX) as the energetic material with varying amounts of porosity and initial pore radii. Table 2 lists the parameters and constants used in the pore collapse model for HMX. All calculations in this section were conducted using a shock pressure of 2.2 GPa. For all simulations, the pore was initially filled with oxygen at atmospheric pressure and at a temperature of 298 K.

The parameters listed in Table 2 were obtained from various sources in the literature (Massoni et al., 1999, Bonnett and Butler, 1996, Kang et al., 1992). While some parameters have little uncertainty associated with their value (e.g. density), other parameters such as viscosity and yield strength have not been established at high shock pressures. The parameters used here therefore represent the current 'best estimates' for these parameters, however experimental work remains to be done to properly quantify these values. The sublimation law parameters (a_v, n) were obtained from pressurized burning test data in the literature (Atwood et al., 1999, Kubota and Sakamoto, 1989). This data is limited to 350 MPa, which is significantly lower than the shock pressures experienced here. The burn law is therefore an extrapolation of current models and should be updated once high pressure burn data is obtained or an alternative approach is available. The use of burn law data for the sublimation law is an assumption based on the modelling presented by Kang et al. (1992) where an asymptotic deflagration law was used to describe pore surface mass flow. As this approached worked well, it has been replicated here. However, a simplified empirical pressure dependent law is used instead of the asymptotic solution to reduce computational overhead and maintain reasonable accuracy.

Table 2: Parameters used for HMX in viscoplastic pore collapse model.

Parameter	Description	Value
ρ_o	Initial solid phase density	1905 kgm ⁻³
c_s	Solid phase specific heat	1031 Jkg ⁻¹ K ⁻¹
k_s	Solid phase conductivity	0.5016 Wm ⁻¹ K ⁻¹
μ_s	Solid phase viscosity	65 kgm ⁻¹ s ⁻¹
\bar{Y}_s	Solid phase plastic yield strength	200 MPa
T_m	Melting temperature at STP	548 K
β_m	Melting point pressure dependence	1.8×10^{-7} kPa ⁻¹
a_v	Burn law parameter	2.5×10^{-7}
n	Burn law parameter	0.66
γ_g	Gas phase ratio of specific heats	1.4
k_g	Gas phase conductivity	0.0833 Wm ⁻¹ K ⁻¹
E/R	Activation temperature	22000 K
A	Pre-exponential factor	1.93×10^{16} s ⁻¹
α	BKW EOS parameter	0.5
β	BKW EOS parameter	0.16
θ	BKW EOS parameter	400
κ	BKW EOS parameter	10.90978

Figure 3 shows pore collapse results for HMX with an initial porosity of 0.5% and an initial pore radius of 2 mm. The figure shows the pore internal radius collapsing with time under the action of the shock pressure. The gas pressure remains negligible until just prior to the point of minimum pore radius. A rapid rise in gas pressure is then observed which corresponds to the rapid consumption of sublimated HMX from the pore wall. After the rapid rise, the pressure reaches a steady state corresponding to a steady burning period.

Figure 4 shows the pore interface and gas temperature histories for the same test case. The interface and gas temperatures are identical in the early portion of the compression process. Once the melting point is reached at the interface, sublimation begins and the interface temperature remains constant. The gas temperature continues to rise gradually for a short time and then experiences a rapid rise as the HMX is rapidly consumed. The temperature reaches an approximate steady level after 0.225 ms.

Figure 5 illustrates the reaction progress during pore collapse. After sublimation begins, HMX begins to build in the gas phase inside the pore. As the pore collapses, the thermodynamic conditions within the pore change until a thermal explosion occurs. This is indicated in Fig. 5 by the rapid decline in HMX mass fraction and the rapid rise in nitrogen (product) mass fraction. Once this condition has been reached, the mass fraction of HMX in the pore remains very small, indicating that the reaction is controlled by the pressure dependent sublimation process at the surface of the pore, rather than the temperature dependent chemical kinetics within the pore.

Figures 6-10 compare viscoplastic pore collapse results for HMX with varying porosity ($\phi = 0.5 - 3\%$) but with a constant initial pore radius of 2 μ m. As can be seen from the figures, changing the porosity while maintaining the initial pore size results in only minor

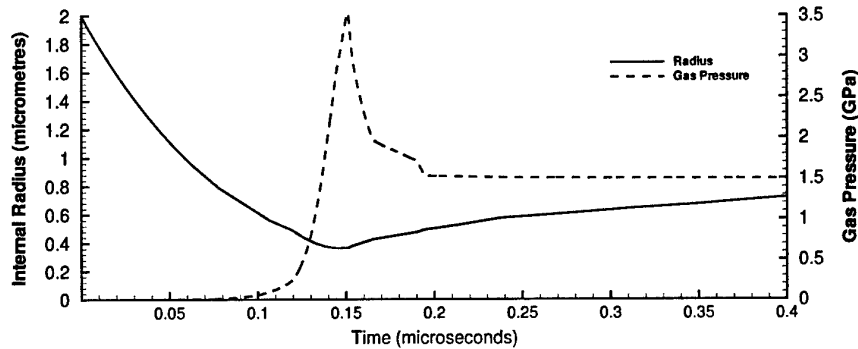


Figure 3: Viscoplastic pore collapse results for HMX - internal pore radius and gas pressure history. $P_s = 2.2$ GPa, $\phi = 0.5\%$ and $a_o = 2.0$ μm .

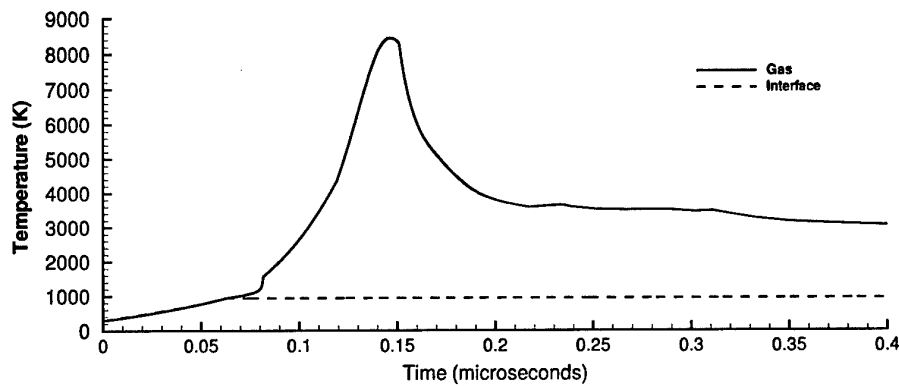


Figure 4: Viscoplastic pore collapse results for HMX - interface and gas temperature history. $P_s = 2.2$ GPa, $\phi = 0.5\%$ and $a_o = 2.0$ μm .

changes in the collapse dynamics and thermodynamic conditions.

Figures 11-15 again compare results from the viscoplastic pore collapse model. For these calculations, the porosity is maintained at 1.5% and the initial pore radius is reduced from 2 to 0.5 μm . The effect of reducing the pore radius has a more significant effect on the collapse dynamics. The maximum explosion temperature (the peaks in Fig. 13) decreases as the pore radius is decreased however the time of thermal explosion increases. The steady-state burn temperature is achieved more quickly with a smaller initial pore radius. The peak HMX mass fraction in the pore gas increases and occurs at a later time as the initial pore radius is decreased.

By examining Eq. 3 and following the arguments presented by Bonnett and Butler (1996), the viscous term resisting the pore collapse motion increases in magnitude as the initial pore size decreases. Therefore as the initial pore size decreases, the collapse rate is decreased and the overall viscoplastic and gas heating mechanisms are reduced. This in

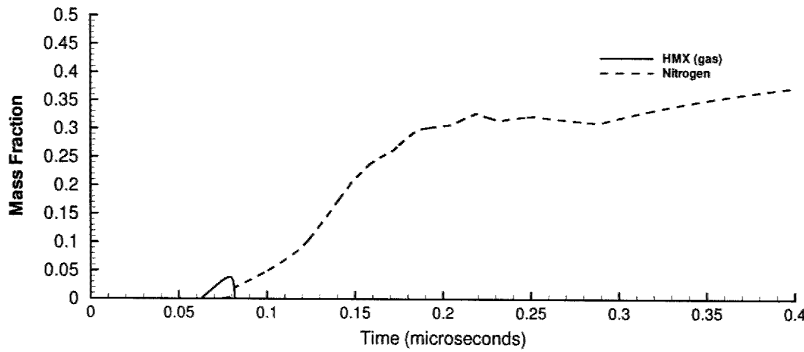


Figure 5: Viscoplastic pore collapse results for HMX - reaction history. $P_s = 2.2$ GPa, $\phi = 0.5\%$ and $a_o = 2.0$ μm .

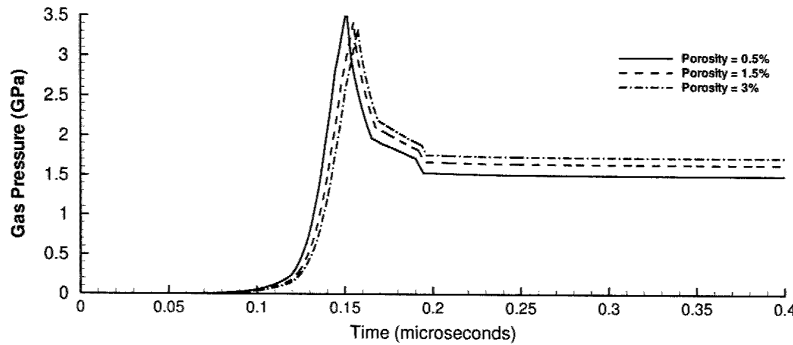


Figure 6: Comparison of pore collapse gas pressure results for HMX. $P_s = 2.2$ GPa, $\phi = 0.5 - 3\%$ and $a_o = 2.0$ μm .

turn reduces the maximum temperatures and extends the point where thermal explosion occurs. Interestingly, the time where the pore radius reaches a minimum (Fig. 12) is only affected slightly by the change in initial pore radius. As the time where the peak pressure occurs (Fig. 11) is only slightly affected, the time where the pore begins to expand remains approximately the same.

3 Reactive Flow Model

3.1 Model Description

The results obtained from the viscoplastic pore collapse model indicate that after an initial transient combustion event (thermal explosion), the pressure and temperature approach a steady state almost immediately after the minimum pore radius is reached. The constant conditions and low mass fraction of HMX in the pore gas indicate that

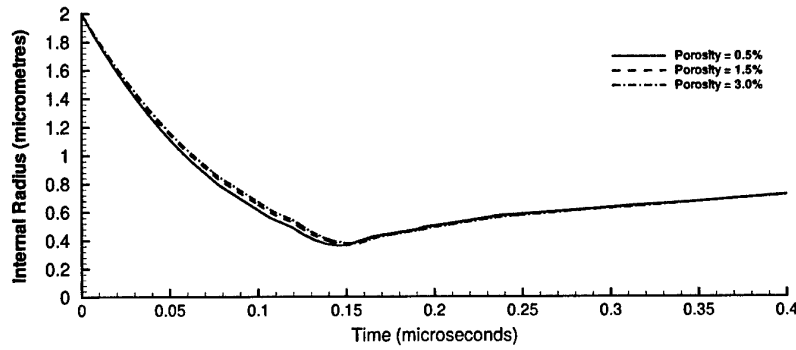


Figure 7: Comparison of pore collapse internal radius results for HMX. $P_s = 2.2$ GPa, $\phi = 0.5$ 3% and $a_o = 2.0$ μm .

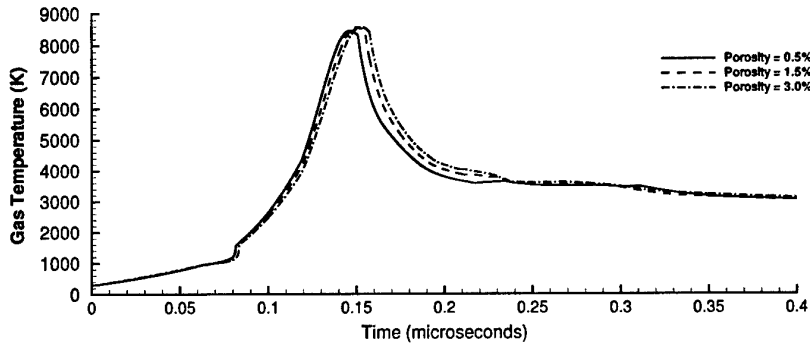


Figure 8: Comparison of pore collapse gas temperature results for HMX. $P_s = 2.2$ GPa, $\phi = 0.5$ 3% and $a_o = 2.0$ μm .

the rate of combustion is controlled by the pressure-dependent sublimation from the pore surface. The results also indicate that the steady state pore gas pressure is approximately the applied shock pressure.

These results can be used to develop a reactive flow model for incorporation into a Eulerian hydrocode. The one-dimensional Euler equations written in conservative form are,

$$\begin{aligned} \frac{\partial \rho}{\partial t} + \frac{\partial \rho u}{\partial x} &= 0 \\ \frac{\partial \rho u}{\partial t} + \frac{\partial (\rho u^2 + P)}{\partial x} &= 0 \\ \frac{\partial \rho E}{\partial t} + \frac{\partial (\rho u E + P u)}{\partial x} &= 0. \end{aligned} \quad (20)$$

These equations are solved using an existing multi-material Eulerian hydrocode de-

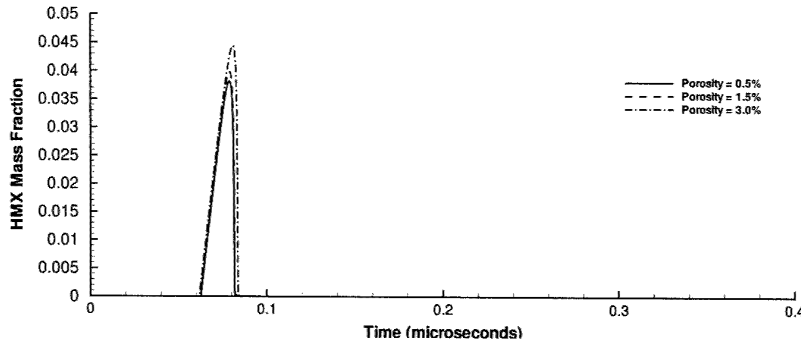


Figure 9: Comparison of pore collapse HMX mass fraction results. $P_s = 2.2$ GPa, $\phi = 0.5 - 3\%$ and $a_o = 2.0$ μm .

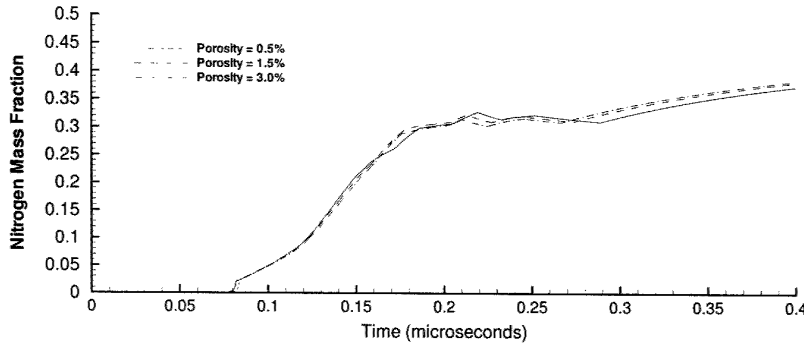


Figure 10: Comparison of pore collapse nitrogen mass fraction results. $P_s = 2.2$ GPa, $\phi = 0.5 - 3\%$ and $a_o = 2.0$ μm .

veloped within WSD (Jones et al., 1998). This two-dimensional code solves the Euler equations using the flux corrected transport algorithm (Oran and Boris, 1987). Various equations of state can be used, however, for the work presented here, the JWL (Lee et al., 1968) equation of state is used for reactive materials (separate forms for un-reacted and reacted components) and the Mie-Gruneisen (Cheret, 1993) equation of state for non-reactive materials. Interface tracking between materials (such as the projectile/explosive interface) is performed using Youngs method (Youngs, 1982).

Assuming pore burning occurs at a pressure equal to the applied shock pressure, the evolution of the porosity after ignition can be described using the following equation (shown in one-dimensional form),

$$\frac{\partial \rho \phi}{\partial t} + \frac{\partial \rho \phi u}{\partial x} = \rho \frac{d\phi}{dt}. \quad (21)$$

This equation convects the porosity as the shock wave processes the material. The right hand side represents burning of the material through porosity change. This term can be calculated three ways. The first represents the case where there is no burning. This

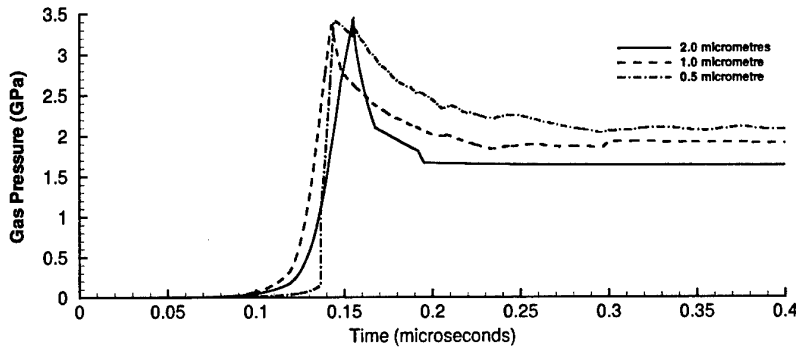


Figure 11: Comparison of pore collapse gas pressure results for HMX. $P_s = 2.2$ GPa, $\phi = 1.5\%$ and $a_o = 0.5 - 2.0 \mu m$.

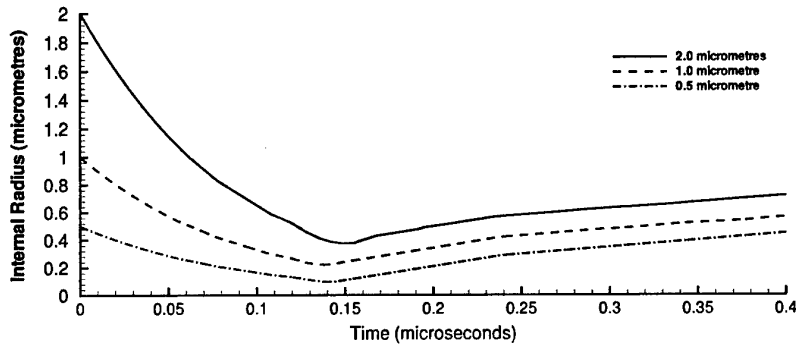


Figure 12: Comparison of pore collapse internal radius results for HMX. $P_s = 2.2$ GPa, $\phi = 1.5\%$ and $a_o = 0.5 - 2.0 \mu m$.

can occur either if the initial shock pressure is too low or in the period before ignition during viscoplastic pore collapse. This first case is represented by,

$$\frac{d\phi}{dt} = 0 \quad f < 1.0 \quad (\text{no ignition}). \quad (22)$$

An Induction Parameter Model is used to determine when to start the internal burning within the pores, where f is the induction parameter. Induction Parameter Models have been used previously to represent the chemical induction time of kinetically complex, supersonic reacting mixtures such as gaseous detonation waves (e.g. Sichel et al., 2002). In the present work, the induction parameter is used to represent the time when a burning pore reaches its minimum radius. Following the viscoplastic pore collapse results, evolution of the porosity from this time onwards is controlled by sublimation from the pore surface. Hence, the induction parameter contains the material response as well as the chemical reaction information.

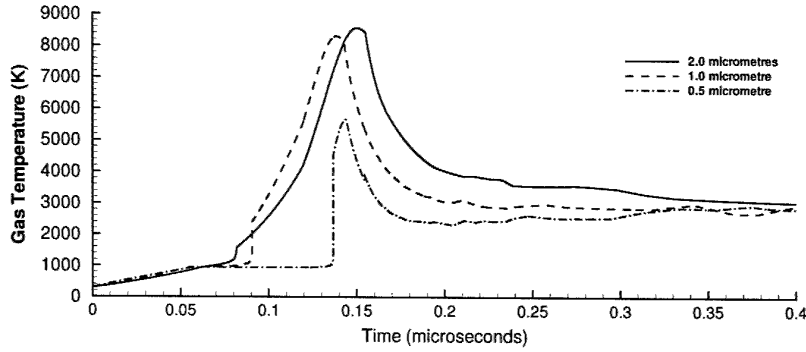


Figure 13: Comparison of pore collapse gas temperature results for HMX. $P_s = 2.2$ GPa, $\phi = 1.5\%$ and $a_o = 0.5 \quad 2.0 \mu m$.

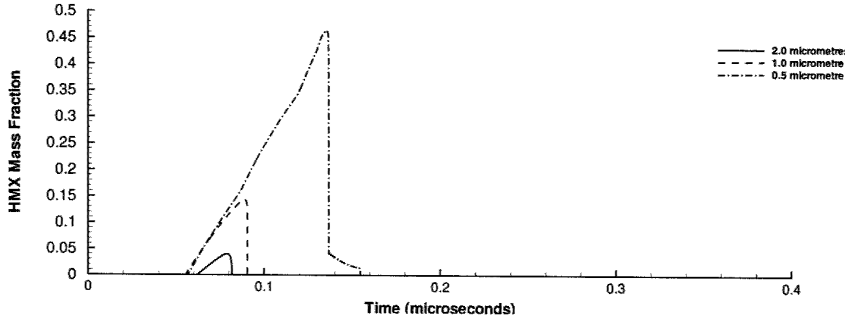


Figure 14: Comparison of pore collapse HMX mass fraction results. $P_s = 2.2$ GPa, $\phi = 1.5\%$ and $a_o = 0.5 \quad 2.0 \mu m$.

Initially, the induction parameter is set to zero throughout the energetic material and is convected using the equation,

$$\frac{\partial \rho f}{\partial t} + \frac{\partial \rho f u}{\partial x} = \frac{\rho}{\tau}, \quad (23)$$

where τ is the induction time calculated from the viscoplastic pore collapse model. It would be very computationally demanding if the induction time were to be calculated for each cell, at every time step using the full viscoplastic pore collapse model. Fortunately, the induction time can be reduced to an analytical expression, determined from prior computational runs using the viscoplastic pore collapse model.

Figure 16 shows the induction time for HMX calculated using the viscoplastic collapse model. The model was used to calculate the induction time for pore radii varying between 0.5 and 2.0 μm and initial porosity varying between 0.5-3.0%. Figure 16 represents the distillation of 126 computational runs. The symbols represent the mean of the data where the error bars are one standard deviation in the computed results. For most cases, there is only a small variation in the computed results at each shock pressure, reflecting the

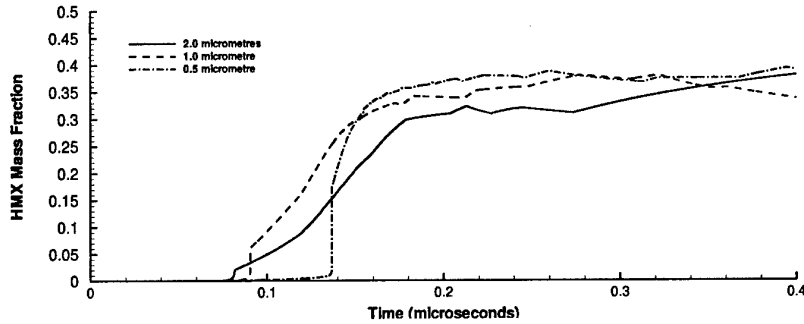


Figure 15: Comparison of pore collapse nitrogen mass fraction results. $P_s = 2.2$ GPa, $\phi = 1.5\%$ and $a_o = 0.5 - 2.0 \mu m$.

viscoplastic pore collapse results presented in the previous section. This variation, denoted by the error bars, becomes larger at small shock pressures and almost insignificant at high shock pressures. In any case, the variation is reasonably small and for the sake of simplicity of the computational model, a power-law curve fit was applied to the mean data (shown in fig. 16). This results in an induction time model for porous HMX,

$$\tau = 0.2173P^{-0.5925}. \quad (24)$$

Equation 24 can be used in Eq. 23 to determine the induction parameter f . In some situations, the applied shock pressure fails to ignite the energetic material. Figure 17 shows the ignition go/no-go curve as calculated by the viscoplastic pore collapse model. If the pressure falls below the curve in Fig. 17 and the induction parameter is less than unity, the energetic material is not expected to ignite. The curve illustrates that the ignitability (not detonability) of the energetic material is inversely proportional to the initial pore radius and only weakly dependent on the porosity at each initial pore radius.

Again, a power-law curve fit was applied to the computed results,

$$P = 0.9710a_o^{0.8842}. \quad (25)$$

During the solution of Eq. 23, Eq. 24 and Eq. 25 are solved to determine the source term (right hand side of Eq. 23). If the pressure is less than the pressure calculated by Eq. 25, then the shock pressure is too low to cause ignition and the source term is set to zero (or the induction time is set to infinity). Otherwise, Eq. 24 is used to determine the induction time and used in the source term of Eq. 23.

Referring to Eq. 21, the right hand source term needs to be evaluated once ignition has begun (i.e. when $f > 1.0$). Burning occurs initially on the inside of the pore surface. After a certain amount of time, the burning changes from an internal surface burn, to an external surface burn. This happens when the energetic material dislocates and hot gas escapes from the pore to become the medium in which individual grains are burning. Shock initiation pressure records (Massoni et al., 1999) show that only a change in the burning mode can explain the observed curvature of the pressure response. Since detailed

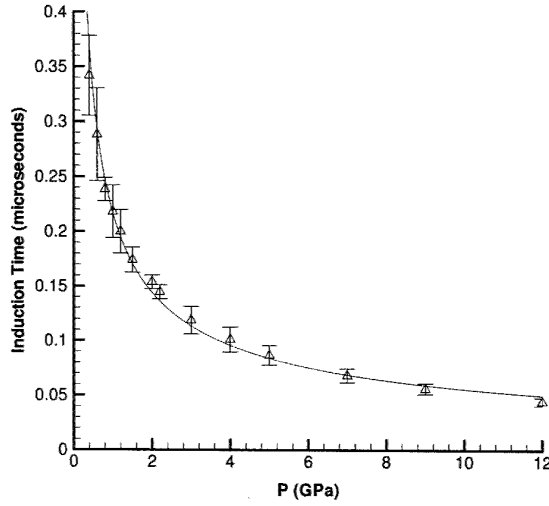


Figure 16: Induction time (τ) versus Shock Pressure for HMX, $\phi = 0.5$ 3.0% and $a_o = 0.5$ 2.0 μm . Error bars indicate one standard deviation in computed results. Red line is a power law curve fit.

observation of when the change in burning occurs is impossible, it is assumed that it occurs at the 'fluidisation limit' (Lee and Tarver, 1980, Massoni et al., 1999) which is defined as the maximum relative volume of a compact bed of spheres and corresponds to $f = 0.24$.

There are two different source terms for Eq. 21 depending on the burning mode. These are (for $f \geq 1.0$),

$$\begin{aligned} \frac{d\phi}{dt} &= N_{pore} S_p a_v P^n & \phi \leq 0.24 \text{ (internal pore burning)} \\ \frac{d\phi}{dt} &= N_{part} S_m a_v P^n & \phi > 0.24 \text{ (external pore burning)}, \end{aligned} \quad (26)$$

where N_{pore} is the number of pores per unit volume, N_{part} is the number of particles per unit volume, S_p and S_m are the pore and particle surface areas respectively and a_v and n are the sublimation parameters used in the viscoplastic pore collapse model. In order to determine the surface areas, the current pore or particle radius must be known. These values are calculated using the following expressions,

$$\begin{aligned} a &= \left(\frac{3\phi}{4\pi N_{pore}} \right)^{\frac{1}{3}} \\ R_{part} &= \left(\frac{3(1-\phi)}{4\pi N_{part}} \right)^{\frac{1}{3}}, \end{aligned} \quad (27)$$

where a is the pore radius and R_{part} is the particle radius.

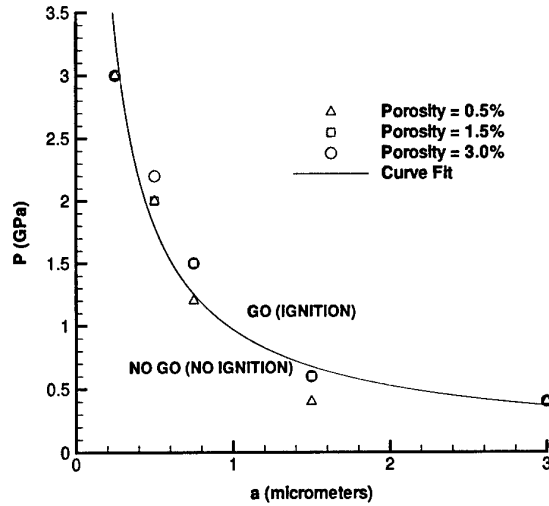


Figure 17: Go/no-go ignitability curve for HMX as calculated by the viscoplastic pore collapse model.

The pore and particle concentrations must be conserved during processing by the shock wave. Solving the following conservation equations ensures this,

$$\begin{aligned}\frac{\partial N_{pore}}{\partial t} + \frac{\partial u N_{pore}}{\partial x} &= 0 \\ \frac{\partial N_{part}}{\partial t} + \frac{\partial u N_{part}}{\partial x} &= 0.\end{aligned}\quad (28)$$

Initially the pore and particle concentrations are uniformly set throughout the energetic material. These initial values are set by using the expressions shown in Eq. 27 and assuming an initial pore radius, porosity and particle size. The initial porosity used in Eq. 27 is the porosity achieved after shock compression when the pore radius is at a minimum. In general, this porosity is approximately one-hundredth the porosity of the pre-shocked material.

An equation of state is now required to close the system of equations. As mentioned previously, the Jones-Wilkins-Lee (JWL) equation of state is used for energetic materials for the present work. The JWL equation of state takes the following form,

$$P = Ae^{-R_1 V} + Be^{-R_2 V} + \frac{\omega C_v T}{V}, \quad (29)$$

where V is the relative volume, T is the temperature and A, B, R_1, R_2, ω (the Gruneisen coefficient) and C_v (the average heat capacity) are constants. There are two sets of constants for the JWL equation for each energetic material, one for the unreacted state and one for the reacted state (or products). Solving the JWL for a reacting mixture therefore

requires knowledge of the mixture fraction and a mixing law. Typically, the mixture fraction is obtained using the Lee and Tarver (1980) Ignition and Growth model Eq. 1. For the current reactive flow model, the porosity is the assumed indicator of volume mixture fraction of reacted material (gaseous reaction products). In fact, the definition of porosity is the volume fraction of the gaseous component.

This mixing law assumes that the relative volumes of the gas and solid phases in the energetic material can be described using,

$$\phi v_g + (1 - \phi) v_s = v_{tot}, \quad (30)$$

where v_g , v_s and v_{tot} represent the relative volumes of the gas, solid and mixed phases respectively. The system is then assumed to be in pressure equilibrium and an iterative procedure is followed where the relative volumes of the gas and solid phases are varied in accordance with Eq. 30 until the JWL equation of state (Eq. 29) for each phase computes the same pressure within a specified tolerance.

3.2 One-Dimensional Results

Equations 21-30 were incorporated into the existing Eulerian hydrocode (Jones et al., 1998) and simulations were performed for shock initiation of an energetic composition containing HMX with 1.7% porosity. Numerical results are compared with the experimental results presented by Massoni et al. (1999) who performed shock initiation experiments on a HMX sample whose porosity and microstructure was determined prior to experimentation. Massoni et al. (1999) also used their reactive flow model to simulate this experiment and results were very favourable. Here, the new reactive flow model presented above is used to simulate the same experiments.

The description of the experimental setup in Massoni et al. (1999) is poor as the only details given were a column of HMX with 1.7% porosity was subjected to an impact imparting a 25 kbar initial shock pressure. In order to simulate this, a one dimensional approach was adopted, using a 5 mm thick lexan projectile striking a 25 mm long column of HMX. Figure 18 shows a schematic of the numerical model, showing the locations of the Lagrangian pressure gauges at 4, 7, 10 and 13 mm respectively. Lagrangian pressure gauges were simulated by convecting the initial positions of the gauges in accordance with the instantaneous velocity field. The actual pressure levels were obtained by extrapolating between the cell values either side of the convected gauge location.

A non-reactive Mie-Grneisen equation of state (Meyers, 1994) is used to describe the lexan projectile material. Table 3 lists the parameters used for the equations of state in the numerical model. The HMX JWL equation of state was assumed to be the same as the one derived by Tarver et al. (1993) for LX-10. LX-10 is an energetic composition comprising of 94.5% HMX and 5.5% Viton Binder. It is pressed to 1.6% porosity.

The results of three computational runs are displayed in Fig. 19. These results were calculated using mono-modal and tri-modal initial pore distributions within the material. In order to calculate the initial pore number density, the following expressions were used,

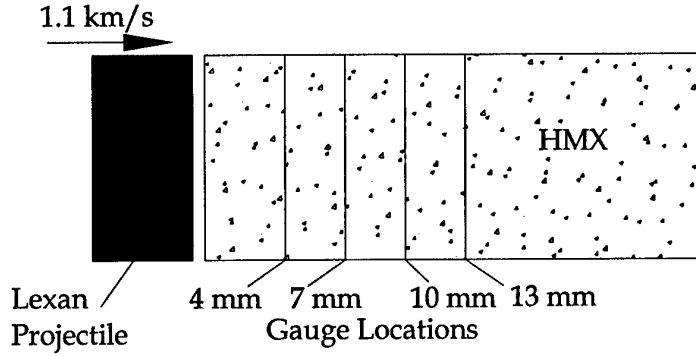


Figure 18: Schematic of one-dimensional numerical shock initiation model for HMX.

$$\begin{aligned}
 N_{pore_i} &= \eta_i N_{pore_T} \\
 N_{pore_T} &= \frac{3\phi}{4\pi} \left(\frac{1}{\sum_{i=1}^{N_p} \eta_i a_{o_i}^3} \right), \quad (31)
 \end{aligned}$$

where the subscript i represents the particular initial pore radius (a_{o_i}), η_i is the fraction of total pores with initial radius a_{o_i} , N_p is the number of pore distributions considered, and the subscript T Reacted JWL represents the total number of pores.

Table 4 shows the initial pore distributions used for the computational runs displayed in Fig. 19. For all runs in Fig. 19, the lexan projectile impact velocity was 1.1 km s^{-1} and 20 computational cells per mm were used to ensure a converged result. A time step of 10^{-9} s was also used. For the external, particle burn model, an initial particle radius of $35 \text{ } \mu\text{m}$ was used for all runs (Massoni et al. 1999).

Table 3: Equation of State Data used in one-dimensional numerical simulations.

Lexan Projectile: Mie-Grüneisen EOS	HMX: Unreacted JWL	HMX: Reacted JWL
$\rho_o = 1.193 \text{ g cm}^{-3}$	$\rho_o = 1.865 \text{ g cm}^{-3}$	
$c_o = 1.933 \text{ km s}^{-1}$	$A = 95220 \text{ GPa}$	$A = 880.7 \text{ GPa}$
$s = 2.04$	$B = 5.944 \text{ GPa}$	$B = 18.36 \text{ GPa}$
$\gamma_o = 0.61$	$R_1 = 14.1$	$R_1 = 4.62$
	$R_2 = 1.41$	$R_2 = 1.32$
	$\omega = 0.8867$	$\omega = 0.38$
	$C_v = 2.7813 \times 10^{-3} \text{ GPa K}^{-1}$	$C_v = 1.0 \times 10^{-3} \text{ GPa K}^{-1}$
	$T_o = 298 \text{ K}$	$E_o = 10.4 \text{ GPa cm}^3 \text{ cm}^{-3} \text{ g}$

The computational results indicate that the shock initiation and associated pressure build-up of HMX is sensitive to the initial pore size distribution within the material.

Table 4: Initial pore distributions for computational runs.

Run (a): Tri-modal	Run (b): Mono-modal	Run (c): Mono-modal
$a_{o1} = 0.5 \mu\text{m} \eta_1 = 0.50$	$a_{o1} = 0.35 \mu\text{m} \eta_1 = 1.0$	$a_{o1} = 0.5 \mu\text{m} \eta_1 = 1.0$
$a_{o2} = 0.35 \mu\text{m} \eta_2 = 0.49$	$a_{o2} = 0 \mu\text{m} \eta_2 = 0$	$a_{o2} = 0 \mu\text{m} \eta_2 = 0$
$a_{o3} = 0.2 \mu\text{m} \eta_3 = 0.01$	$a_{o3} = 0 \mu\text{m} \eta_3 = 0$	$a_{o3} = 0 \mu\text{m} \eta_3 = 0$
$N_{p1} = 2.4276 \times 10^{10} \text{ cm}^{-3}$	$N_{p1} = 9.4658 \times 10^{10} \text{ cm}^{-3}$	$N_{p1} = 3.2468 \times 10^{10} \text{ cm}^{-3}$
$N_{p2} = 2.3791 \times 10^{10} \text{ cm}^{-3}$	$N_{p2} = 0$	$N_{p2} = 0$
$N_{p3} = 4.8553 \times 10^8 \text{ cm}^{-3}$	$N_{p3} = 0$	$N_{p3} = 0$
$R_{part_o} = 35 \mu\text{m}$	$R_{part_o} = 35 \mu\text{m}$	$R_{part_o} = 35 \mu\text{m}$

Fig. 19(a) shows reasonable agreement between the computational model and the experimental results. The correct shock speeds are computed along with the initial pressure rises. The peak pressure for the gauge at 13 mm is under-predicted, however this does not seem to affect the run-to-detonation distance (shown later). When the simulation is repeated with a mono-modal initial pore distribution of $0.35 \mu\text{m}$ (Fig. 19(b)), the simulated pressure build up occurs much more quickly with an associated transition to detonation observed. Similarly, when the mono-modal initial pore size is increased to $0.5 \mu\text{m}$ (Fig. 19(c)), a slower pressure build-up occurs. In this case, excellent comparisons are observed for the gauges located at 4 mm and 7 mm, however reaction rates are too slow to maintain the pressure rises for the gauges at 10 mm and 13 mm.

These results reach the same conclusions as the study by Massoni et al. (1999) in that to model the shock initiation of energetic materials accurately, a good knowledge of the microstructure, mechanical and chemical properties is necessary. In the study by Massoni et al. (1999), a tri-modal initial pore radius distribution of 60% $0.5 \mu\text{m}$, 39% $0.2 \mu\text{m}$ and 1% $0.15 \mu\text{m}$ was found to model the shock initiation. This (small) difference in pore distribution can probably be attributed to the differences in the viscoplastic pore collapse models used in the two studies. Here, a different reaction mechanism and combustion model was used along with different parameters for the pressure dependent burn law. A BKW equation of state was also used within the viscoplastic pore collapse model whereas Massoni et al. (1999) use the H9 equation of state. However, despite these differences and the use of a different numerical approach, similar results were obtained albeit with a slightly different pore distribution. The actual pore distribution is difficult to measure and for this particular case, measurements by Massoni et al. (1999) suggest a majority of pores at $0.5 \mu\text{m}$.

As the details of the shock initiation experiment were not extensive, the method of shock generation used in the simulations is not identical to the method used in the experiment. Therefore, the arrival times of the release waves from the free-end of the projectile will differ between computation and experiment. The complete wave system is shown in Fig. 20 which is a space-time (x-t) plot of equally spaced contours of pressure.

The interface between the projectile and the HMX is initially at 0.5 cm. From this point, two initial shock waves are formed in the HMX and projectile respectively, with a region of uniform pressure between the shock waves. As the shock in the HMX processes the material, pores are collapsed and burning begins, resulting in an increase in pressure

and acceleration of shock speed (marked as the Transition region on Fig. 20). Eventually the shock wave transitions to a constant speed detonation wave. Release (or expansion) waves are generated when the initial shock in the projectile is reflected from the free-end. The release waves are transmitted into the HMX and affect the pressure levels after the transitioning shock-to-detonation wave. As the detonation wave travels faster than the release waves, the run-to-detonation distance should not be affected. This is illustrated by Fig. 21, which shows a comparison between the run-to-detonation distance (or pop-plot) measurements of Vanpoperynghe et al. (1985) and the numerical model. Following Massoni et al. (1999), the run-to-detonation distance was taken to be the distance along the explosive where the slope of the shock wave changes on a space-time ($x-t$) plot. Initial shock pressures were varied in the simulations by changing the impact speed of the lexan projectile. The experimental measurements are represented by a linear relationship between $\log h$ and $\log P$. The energetic composition used by Vanpoperynghe et al. (1985) was 96% HMX and it is assumed here to have a porosity of approximately 1.7%. The comparison between experiment and calculation is reasonably good.

In order to investigate the effects of porosity on shock sensitivity, two simulations were performed using the tri-modal pore pore distribution used in Fig. 19(a) but with porosities of 0.5% and 3%. As expected, the porosity level has a significant effect on shock sensitivity, with a reduction in sensitivity observed for the lower porosity level. A similar change in sensitivity can also be observed when the porosity is kept constant, but the tri-modal distribution is changed. Figure 23 illustrates this effect, showing a decrease in sensitivity when the average initial pore size is increased and vice-versa when the average pore size is decreased. This can be explained in terms of the available surface area for combustion. Provided that the shock pressure is high enough for ignition to occur at the pore locations (see Fig. 17), the smaller pore radii allow a higher surface area for combustion to occur and hence an increase in sensitivity is observed. There is a limit to how much the sensitivity can be increased by reducing the pore radii and this is given by Fig. 17 using the viscoplastic pore collapse model.

3.3 Two-Dimensional Results

In order to demonstrate the capabilities of the reactive flow model and Eulerian code the single fragment impact experiment (as described by Collignon et al., 1992) was simulated using the HMX model described previously in this report.

Two-dimensional, axisymmetric simulations were performed using the procedure outlined above. The full set of equations used for the axisymmetric (cylindrical) case is,

$$\begin{aligned}
 \frac{\partial \rho}{\partial t} + \frac{\partial \rho u}{\partial x} + \frac{1}{r} \frac{\partial r \rho v}{\partial r} &= 0 \\
 \frac{\partial \rho u}{\partial t} + \frac{\partial (\rho u^2 + P)}{\partial x} + \frac{1}{r} \frac{\partial r \rho uv}{\partial r} &= 0 \\
 \frac{\partial \rho v}{\partial t} + \frac{\partial \rho uv}{\partial x} + \frac{1}{r} \frac{\partial r (\rho v^2 + P)}{\partial r} &= 0 \\
 \frac{\partial \rho E}{\partial t} + \frac{\partial (\rho u E + P u)}{\partial x} + \frac{1}{r} \frac{\partial r (\rho v E + P v)}{\partial r} &= 0
 \end{aligned}$$

$$\begin{aligned}
\frac{\partial \rho \phi}{\partial t} + \frac{\partial \rho \phi u}{\partial x} + \frac{1}{r} \frac{\partial r \rho \phi v}{\partial r} &= \rho \frac{d\phi}{dt} \\
\frac{\partial \rho f}{\partial t} + \frac{\partial \rho f u}{\partial x} + \frac{1}{r} \frac{\partial r \rho f v}{\partial r} &= \frac{\rho}{\tau} \\
\frac{\partial N_{pore}}{\partial t} + \frac{\partial N_{pore} u}{\partial x} + \frac{1}{r} \frac{\partial r N_{pore} v}{\partial r} &= 0 \\
\frac{\partial N_{part}}{\partial t} + \frac{\partial N_{part} u}{\partial x} + \frac{1}{r} \frac{\partial r N_{part} v}{\partial r} &= 0
\end{aligned}$$

where r is the radius from the axis and v is the radial velocity. The source terms are as described earlier in this report.

A schematic representing the single fragment impact test is shown in Fig. 24. Here a 14.32 mm diameter steel projectile (representing a fragment) travelling at 847 ms⁻¹ strikes a 76.2 mm diameter sample of HMX within a 6.35 mm thick aluminium casing and coverplate. As the model is axisymmetric, only half of the system needs to be represented. A reflective boundary condition is imposed on the centreline to simulate the other half of the material. Transmissive boundary conditions are imposed on other boundaries of the model. An ordered mesh is used with 4 cells per mm in the x-direction and r-directions in conjunction with a time-step of 1.5×10^{-9} s. A Mie-Gruneisen equation of state was used for the steel projectile and aluminium casing (parameters from Meyers, 1994) and the JWL equation of state shown in Table 3 was used for the energetic material.

In the experiments performed by Collignon et al. (1992), various HMX based formulations were tested. For the purposes of simulation, it was decided that the formulation LX-14(N) was closest to the HMX model derived in this report. This formulation consists of 95.5% HMX and 4.5% estane binder. However, no information on the microstructure (i.e. porosity level and pore size distribution) is available therefore the trimodal initial pore distribution used in the previous section is used for this simulation. The impact speed of 847 ms⁻¹ was determined experimentally as the lowest fragment impact velocity that caused the explosive to detonate.

Figure 25 shows results from the two dimensional simulation of the single fragment impact test. In each figure, contours of pressure (top half) and contours of fraction of reacted explosive (lower half) are shown in order to illustrate the processes occurring within the energetic material. Initially (Fig. 25(a)), a relatively mild shock wave is imparted to the explosive after passing through the aluminium coverplate. Reactions are initiated as shown by the well-spaced contours of reacted explosive. Later in time (Fig. 25(b)), the shock wave strength increases due to the quickening reactions behind it. Eventually the shock wave transitions into a detonation wave (Fig. 25(c)), which is evident by the defined high pressure detonation front and the concentrated reaction zone. The detonation wave eventually reflects from the outer aluminium case (Fig. 25(d)), deforming it in its wake.

Thus, the implementation of the reactive flow model into the two-dimensional hydrocode represents a significant, new capability for Weapons Systems Division. The Induction-Parameter-Model allows a computationally efficient approach of using a mechanistic reactive flow model for multi-dimensional simulations. Therefore the combined effects of microstructure, casing and fragment impact geometry can be explored and give meaningful results for those involved in Insensitive-Munitions hazard assessments.

4 Summary, Conclusions and Future Work

A reactive flow model has been developed based upon a viscoplastic pore collapse model for hot spot generation. The viscoplastic pore collapse model represents an extension of the model proposed by Kang et al. (1992) and subsequently developed by Bonnet and Butler (1996) and Massoni et al. (1999). Results from the viscoplastic pore collapse model indicate that pore collapse is more sensitive to changes in initial pore radius rather than bulk porosity levels. The model also shows that during collapse, ignition begins with a thermal explosion inside the pore that quickly develops into a quasi-steady burning process that occurs approximately at the shock pressure.

Using this information, a reactive flow model was developed using a similar framework to Massoni et al. (1999) but using a more computationally efficient Induction-Parameter-Model which is used to simulate the initial shock collapse and ignition time of the pores in the energetic material. The Induction-Parameter-Model therefore represents the mechanical and reactive properties of the material during pore collapse. The reactive flow model was imbedded in an existing Eulerian hydrocode and used for one and two-dimensional shock initiation simulations in HMX. One-dimensional simulations are directly compared with experimental results and show that the initial distribution of pores is important to accurately simulate the shock initiation process. There is also reasonable agreement with the run-to-detonation distance results of Vanpoperinghe (1985).

An example of a two-dimensional simulation is presented for the single fragment impact test. The results show a prompt shock detonation initiation occurs for the particular projectile diameter and impact velocity and illustrates the hydrocode's capability for determining the interaction of energetic material microstructure, wave structure, casing material and fragment impact geometry. Two-dimensional simulations are made possible on the current WSD computer system by using the Induction-Parameter-Model as it significantly reduces the computational cost compared with the full implementation of the viscoplastic pore collapse model.

Improvements can be made to the reactive flow model. The pressure dependent burn model is extrapolated well beyond the pressure range of the experiments it was determined from. It is difficult to imagine a constant pressure burn experiment being devised in the near future that can operate at detonation pressures and give the parameters required for the burn model. Instead, a better approach would be to include the chemical kinetics into the viscoplastic pore collapse model and the reactive flow model. Tarver et al. (1996) provide a three-step chemical decomposition model for HMX that involves reactions in the solid and gaseous phases (including a phase change step). This model can be implemented to improve the accuracy of the models. Further improvements include a more rigorous treatment of the phase change during melting and obtaining more accurate mechanical property data at high shock pressures. Also, accurate multiple shock simulations are not possible using the present formulation. A conductive heat loss model for the collapsing pores needs to be implemented within the hydrocode before this is possible.

A new gas gun facility (Doolan, 2001) is nearing completion at Weapons Systems Division that will provide new experimental data to compare with the reactive flow model. It is also hoped that the facility will be able to provide better estimates of mechanical data such as yield strength and viscosity. Incorporating damage and aging models would also

be useful. Such models could predict the changes in porosity and physical properties experienced during mechanical insults and the natural aging process in order to determine the changes in shock sensitivity during the service-life of the weapon or if damaged during combat or handling.

5 References

Anderson, A.B., Ginsburg, M.J., Seitz and Wackerle, J. 'Shock Initiation of Porous TATB', 7th Symposium (International) on Detonation, 1981, pp. 385-392.

Atwood, A.I., Boggs, T.L., Curran, P.O., Parr, T.P., Hanson-Parr, D.M., Price, C.F. and Wiknich, J. 'Burning Rate of Solid Propellant Ingredients, Part 1: Pressure and Initial Temperature Effects', Journal of Propulsion and Power, Vol. 15, No. 6, 1999, pp 740-747.

Baer, M.R., Kipp, M.E. and van Swol, F. 'Micromechanical Modelling of Heterogeneous Energetic Materials', 11th Symposium (International) on Detonation, 1998, pp. 788-797.

Bennett, L.S. 'Constitutive Modelling of Weak and Strong Shock-Initiation of Porous Explosives', 11th Symposium (International) on Detonation, 1998, pp. 612-620.

Bonnett, D.L. and Butler, P.B. 'Hot-Spot Ignition of Condensed Phase Energetic Materials', Journal of Propulsion and Power, Vol. 12, No. 4, July-Aug, 1996. Bowden, F.P. and Yoffe, A.D. 'Initiation and Growth of Explosion in Liquids and Solids', Cambridge University Press, London, 1952.

Carroll, M.M. and Holt, A.C. 'Static and Dynamic Pore-Collapse Relations for Ductile Porous Materials', Journal of Applied Physics, Vol. 43, No. 4, 1972, pp. 1626-1637.

Chaudri, M.M. 'The Initiation of Fast Decomposition in Solid Explosives by Fracture, Plastic Flow, Friction and Collapsing Voids', 9th Symposium (International) on Detonation, 1989, pp. 331-339.

Cheret, R. 'Detonation of Condensed Explosives', Springer-Verlag, New York, 1993.

S.L. Collignon, W.P. Burgess, W.H. Wilson and K.D. Gibson, 'Insensitive Munitions Program for the Development and Evaluation of Metal Accelerating Explosives', ADPA-IMTS92, 1992, pp.136-158.

Conely, P.A., Benson, D.J. and Howe, P.M. 'Microstructural Effects in Shock Initiation', 11th Symposium (International) on Detonation, 1998, pp. 768-780.

Cook, M.D., Haskins, P.J. and Stennett, C. 'Development and Implementation of an Ignition and Growth Model for Homogeneous and Heterogeneous Explosives', 11th Symposium (International) on Detonation, 1998, pp. 589-598.

Doolan, C.J. 'A Two-Stage Light Gas Gun for the Study of High Speed Impact in Propellants', DSTO Technical Report, DSTO-TR-1092, 2001.

Fried, L. and Howard, M. 'Cheetah Users Manual', UCRL-MA-117541, Lawrence Livermore National Laboratory, USA, 2001.

Frey, R.B. 'Some Aspects of the Micromechanics of Hot Spot Formation in Energetic Materials', Hazard Studies for Solid Propellant Rocket Motors - AGARD Conference Proceedings No. 367, 1984.

Johnson, J.N., Tang, P.K. and Forest, C.A. 'Shock-Wave Initiation of Heterogeneous Reactive Solids', *Journal of Applied Physics*, Vol. 57, No. 9, 1985, pp. 4323-4334.

Jones, D.A., Kemister, G. and Borg, R.A.J., 'Numerical Simulation of Detonation in Condensed Phase Explosives', DSTO Technical Report, DSTO-TR-0705, 1998.

Jones, D.A. and Kennedy, D.L. 'Application of the CPeX Non-Ideal Explosive Model to PBXW-115', MRL Research Report, DSTO, MRL-TR-91-40, 1991.

Kang, J., Butler, P.B. and Baer, M.R. 'A Thermomechanical Analysis of Hot Spot Formation in Condensed-Phase, Energetic Materials', *Combustion and Flame*, Vol. 89, 1992, pp 117-139.

Kasainov, B.A., Borisov, A.A., Ermolaev, B.S. and Korotkov, A.I. 'Two-Phase Visco-Plastic Model of Shock Initiation of Detonation in High Explosives', 7th Symposium (International) on Detonation, pp. 435-447, 1981.

Kirby, I.J. and Leiper, G.A. 'A Small Divergent Theory for Intermolecular Explosives', 8th Symposium (International) on Detonation, pp. 176-186, 1985.

Kubota, N. and Sakamoto, S. 'Combustion Mechanism of HMX', *Propellants, Explosives, Pyrotechnics*, Vol. 14, 1989, pp. 6-11.

Lee, E.L., Hornig, H.C. and Kurry, J.W. 'Adiabatic Expansion of High Explosive Detonation Products', Lawrence Livermore Laboratory Report UCRL-50422, 1968.

Lee, E.L. and Tarver, C.M., 'Phenomenological Model of Shock Initiation in Heterogeneous Explosives', *Physics of Fluids*, Vol. 23, No. 12, 1980, pp. 2362-2372.

Mader, C.L., 'Numerical modelling of explosives and propellants', Boca Raton, Fla. : CRC Press, 1998.

Massoni, J., Saurel, R., Baudin, G. and Demol, G. 'A Mechanistic Model for Shock Initiation of Solid Explosive', *Physics of Fluids*, Vol. 11, No. 3, 1999, pp. 710-736.

McBride, B.J. and Gordon, S. 'Fortran IV Program for Calculation of Thermodynamic Data', NASA Technical Note TN-D 4097, NASA, Washington, DC, USA, 1967.

Mellor, A.M., Wiegand, D.A. and Isom, K.B. 'Hot Spot Histories in Energetic Materials', *Combustion and Flame*, Vol. 101, 1995, pp. 26-35.

Meyers, M.A. 'Dynamic Behaviour of Materials', John Wiley and Sons, 1994.

Oran, E.S. and Boris, J.P. 'Numerical Simulation of Reactive Flow', Elsevier Science Publishing, New York, 1987.

Partom, Y. 'A Void Collapse Model for Shock Initiation', 7th Symposium (International) on Detonation, 1981, pp. 506-516.

Partom, Y. and Wackerle, J. 'Surface-Burn Model for Shock Initiation', 9th Symposium (International) on Detonation, 1989, pp. 735-742.

Sichel, M., Tonello, N.A., Oran, E.S. and Jones, D.A. 'A Two-Step Kinetics Model for Numerical Simulation of Explosions and Detonations in H₂-O₂ Mixtures', *Proceedings of the Royal Society London A*, Vol. 458, 2002, pp. 49-82.

Tarver, C.M. and Nichols, A.L. 'Hot Spot Growth in a Thermal-Chemical-Mechanical Reactive Flow Model for Shock Initiation of Solid Explosives', 11th Symposium (International) on Detonation, 1998, pp. 599-605.

Tarver, C.M., Chidester, S.K. and Nichols, A.L. 'Critical Conditions for Impact- and Shock-Induced Hot Spots in Solid Explosive', Journal of Physical Chemistry, Vol. 100, 1996, pp.5794-5799.

Tarver, C.M., Urtiew, P.A. and Tao, W.C. 'Effects of Tandem and Colliding Shock Waves on the Initiation of Triaminotrinitrobenzene', Journal of Applied Physics, Vol. 78, No. 5, 1995, pp. 3089-3095.

Tarver, C.M., Urtiew, P.A., Chidester, S.K. and Green, L.G. 'Shock Compression and Initiation of LX-10', Propellants, Explosives and Pyrotechnics, Vol. 18, 1993, pp. 117-127.

Vanpoperynghe, J., Sorel, J., Aveille, J. and Adenis, J.C. 'Shock Initiation of TATB and HMX Explosive Compositions', 8th Symposium (International) on Detonation, 1985, pp. 892-913. Vaullerain, M. and Espagnacq, A. 'Reparametrization of the BKW Equation of State for the Triazoles and Comparison of the Detonation Properties of HMX, TNMA and NTO by means of Ab-Initio and Semiempirical Calculations', Propellants, Explosives and Pyrotechnics, Vol. 23, 1998, pp. 73-76.

Youngs, D.L. 'Time-Dependent Multi-Material Flow with Large Fluid Distortion', Numerical Methods for Fluid Dynamics, K.W. Morton and M.J. Baines (eds), 1982.

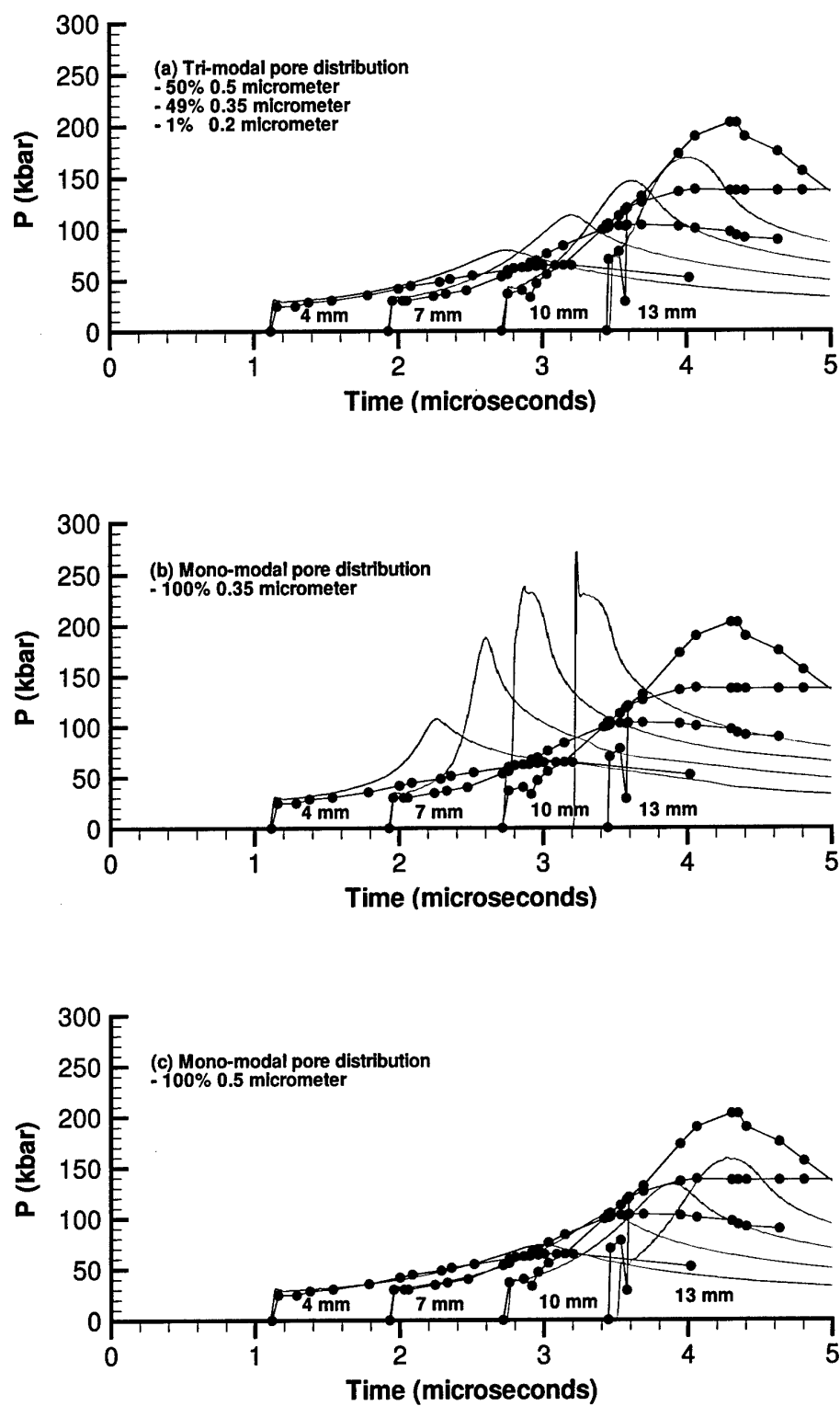


Figure 19: Numerical and experimental pressure records for HMX with 1.7% porosity. Dots represent experimental results while coloured lines indicate numerical results.

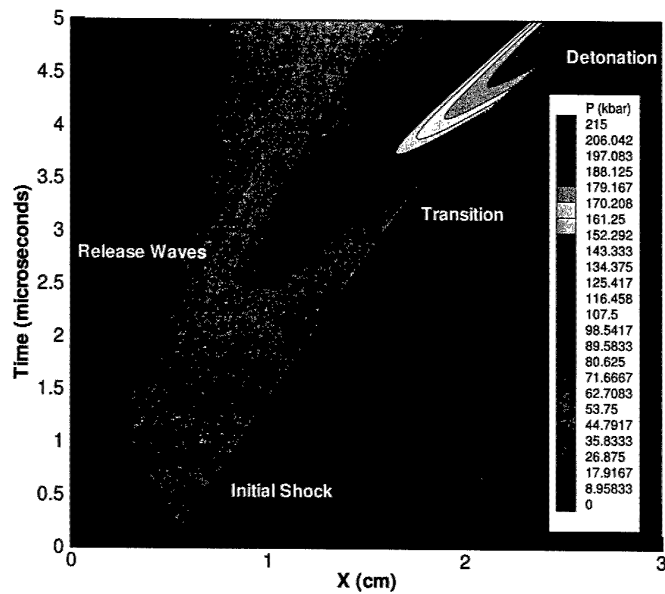


Figure 20: Space-time (x-t) diagram for one dimensional shock initiation simulation of HMX with 1.7% porosity. Contours are equally spaced values of pressure.

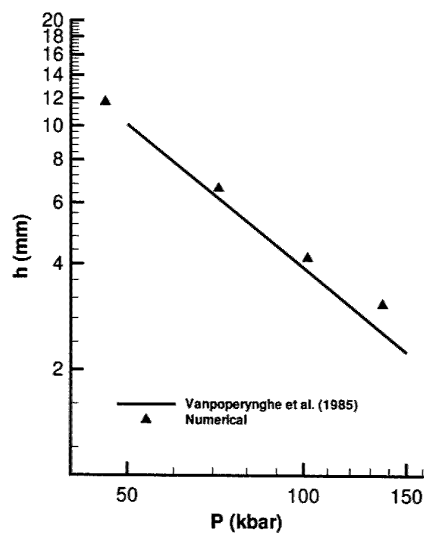


Figure 21: Comparison between numerical and experimental run to detonation distance for HMX with 1.7% porosity.

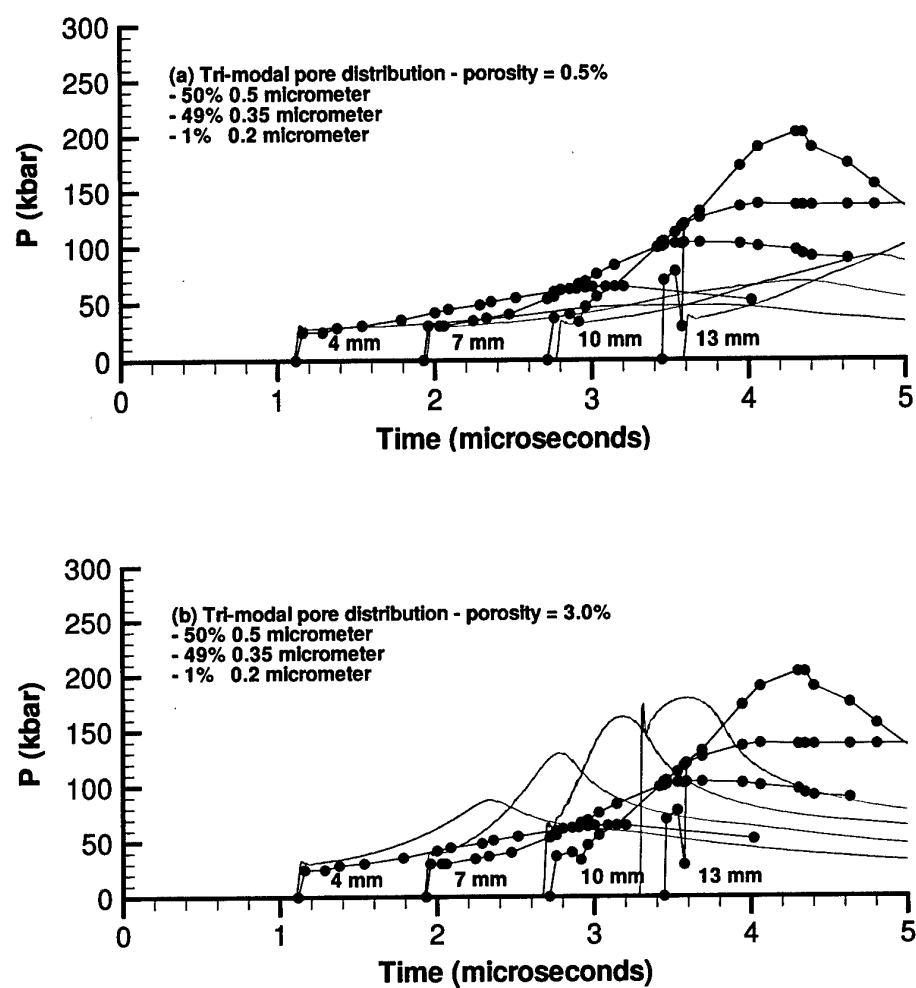


Figure 22: Numerical and experimental pressure records for HMX with varying porosity and a constant tri-modal pore distribution. Dots represent experimental results while coloured lines indicate numerical results.

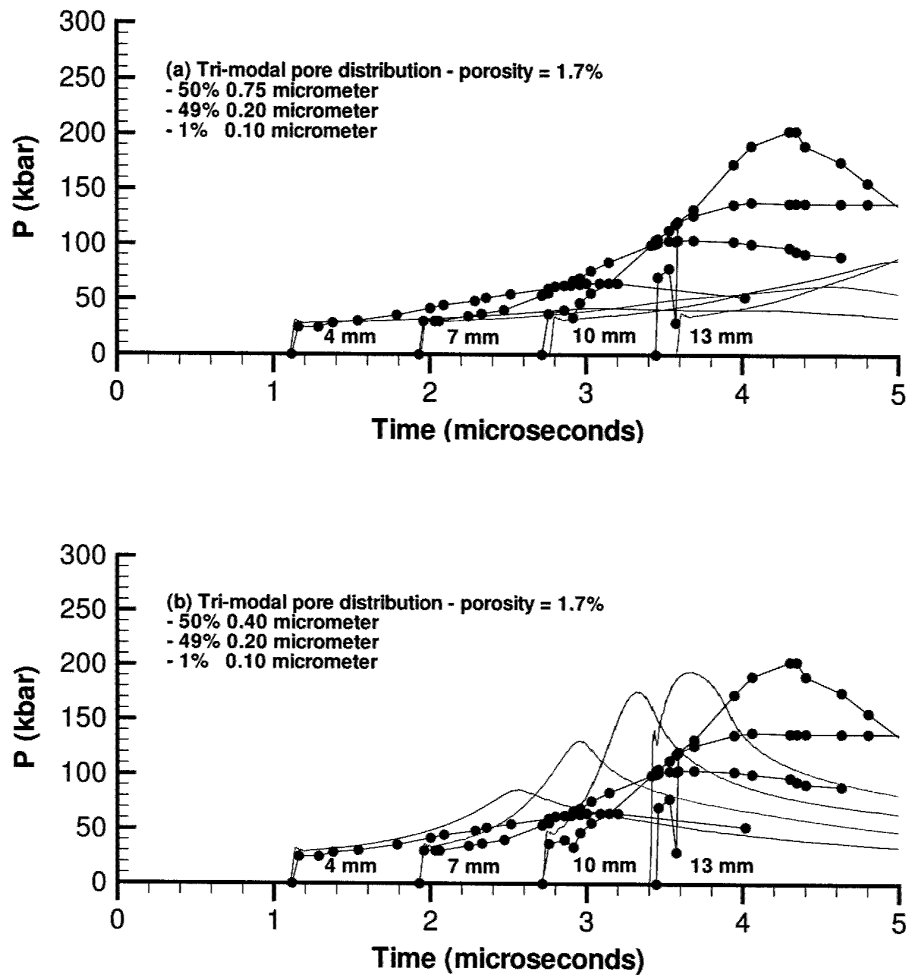


Figure 23: Numerical and experimental pressure records for HMX with constant porosity and a varying tri-modal pore distribution. Dots represent experimental results while coloured lines indicate numerical results.

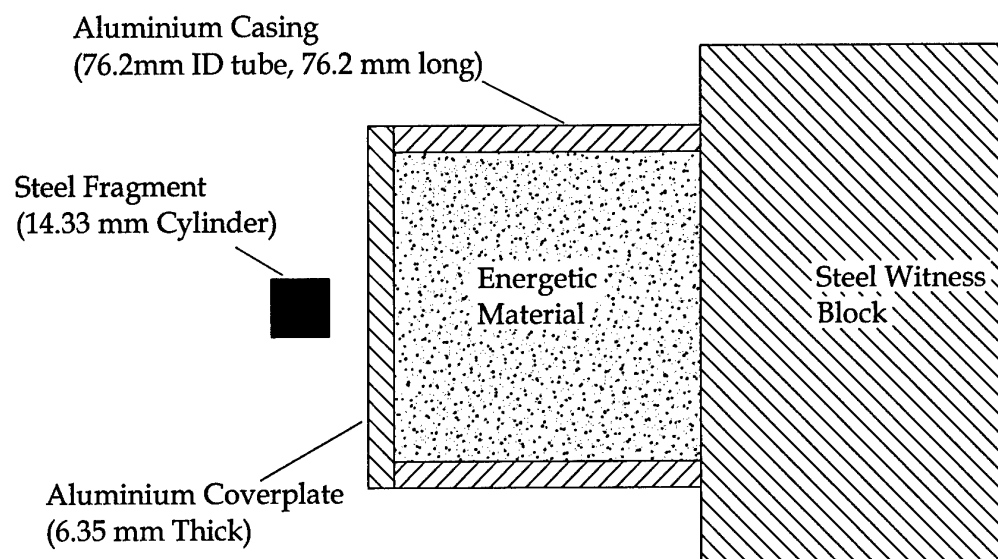


Figure 24: Schematic illustrating single fragment impact test.

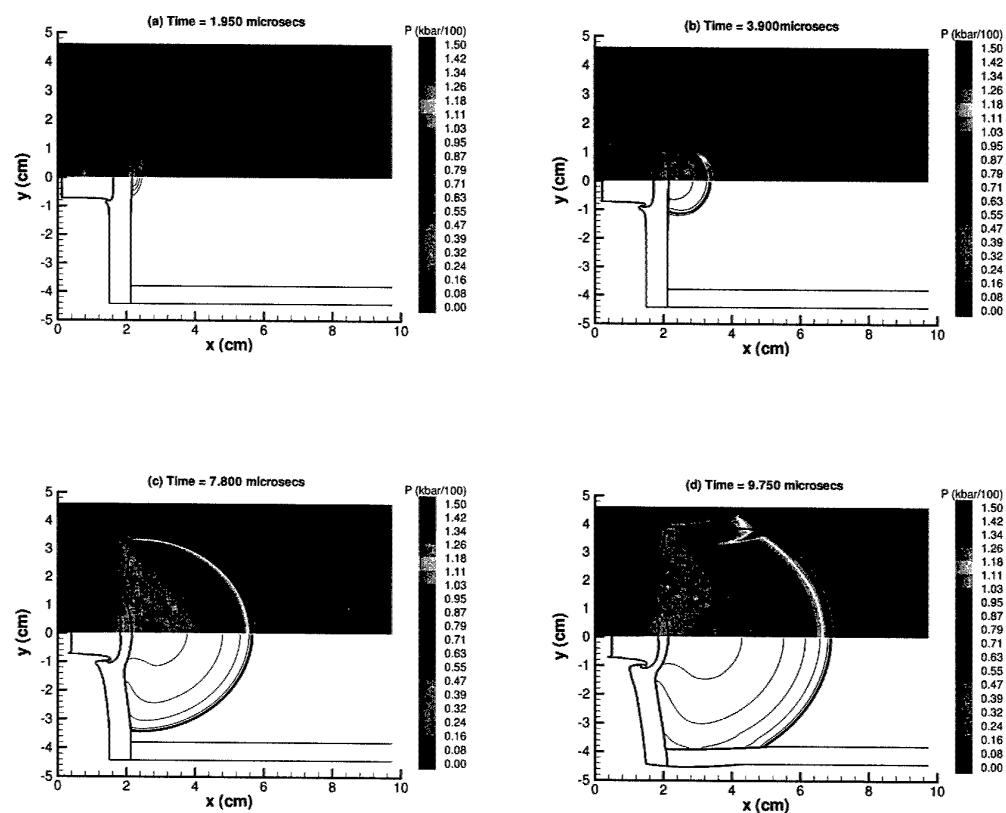


Figure 25: Two-dimensional simulation of single fragment impact test. Results show coloured contours of pressure (top half of results) and equally spaced contours of fraction of reacted explosive (lower half).

Best Available Copy

DSTO-TR-1383

DISTRIBUTION LIST

A Microstructure Dependent Reactive Flow Model for Heterogeneous Energetic Materials

C. J. Doolan

Number of Copies

DEFENCE ORGANISATION

Task Sponsor

DGNAVSYS, Campbell Park, ACT	1
------------------------------	---

S&T Program

Chief Defence Scientist	
FAS Science Policy	
AS Science Corporate Management	
Director General Science Policy Development	
Counsellor, Defence Science, London	Doc Data Sht
Counsellor, Defence Science, Washington	Doc Data Sht
Scientific Adviser to MRDC, Thailand	Doc Data Sht
Scientific Adviser Trials	
Scientific Adviser Policy and Command	
Navy Scientific Adviser	1
Scientific Adviser, Army	Doc Data Sht
Air Force Scientific Adviser	Doc Data Sht
Director Trials	Doc Data Sht

Systems Sciences Laboratory

Chief, WSD	1
RLMWS	1
Head PST Group	1
Task Manager, Dr Con Doolan	1
Author	5

Platforms Sciences Laboratory

Dr David Jones, MPD	1
---------------------	---

DSTO Libraries

Library Edinburgh	2
Australian Archives	1

Capability Development Division

Director General Maritime Development	1
---------------------------------------	---

Knowledge Staff

Director General Command, Control, Communications and Computers (DGC4)	Doc Data Sht
--	--------------

Navy

SO(Science), Director of Naval Warfare, Maritime Headquarters Annex, Garden Island	Doc Data Sht
LCDR A.R. Clark, Armament Systems (Explosive Ordnance), Directorate of Naval Weapon Systems	1

Army

ABCA National Standardisation Officer, Land Warfare Develop- ment Sector, Puckapunyal	4
SO(Science), DJFHQ(L), Milpo, Enoggera, Qld 4057	Doc Data Sht
NAPOC QWG Engineer NBCD c/- DENGERS-A, HQ Engineer Centre Liverpool Military Area, NSW 2174	Doc Data Sht

Intelligence Program

DGSTA Defence Intelligence Organisation	1
Manager, Information Centre, Defence Intelligence Organisa- tion	1

Corporate Support Program (libraries)

Library Manager, DLS-Canberra	Doc Data Sht
Library Manager, DLS-Sydney	Doc Data Sht
Additional copies for DEC for exchange agreements	
US Defense Technical Information Center	2
UK Defence Research Information Centre	2
Canada Defence Scientific Information Service	1
NZ Defence Information Centre	1
National Library of Australia	1

UNIVERSITIES AND COLLEGES

Australian Defence Force Academy Library	1
Head of Aerospace and Mechanical Engineering, ADFA	1
Deakin University Library, Serials Section (M List)	1
Senior Librarian, Hargrave Library, Monash University	Doc Data Sht
Librarian, Flinders University	1

OTHER ORGANISATIONS

NASA (Canberra)	1
-----------------	---

ABSTRACTING AND INFORMATION ORGANISATIONS

INSPEC: Acquisitions Section Institution of Electrical Engi- neers	1
Library, Chemical Abstracts Reference Service	1

Engineering Societies Library, US	1
Materials Information, Cambridge Science Abstracts, US	1
Documents Librarian, The Center for Research Libraries, US	1

INFORMATION EXCHANGE AGREEMENT PARTNERS

Acquisitions Unit, Science Reference and Information Service, UK	1
---	---

SPARES

DSTO Edinburgh Research Library	5
---------------------------------	---

Total number of copies:	48
--------------------------------	-----------

DEFENCE SCIENCE AND TECHNOLOGY ORGANISATION DOCUMENT CONTROL DATA				1. CAVEAT/PRIVACY MARKING	
2. TITLE A Microstructure Dependent Reactive Flow Model for Heterogeneous Energetic Materials			3. SECURITY CLASSIFICATION Document (U) Title (U) Abstract (U)		
4. AUTHOR C. J. Doolan			5. CORPORATE AUTHOR Systems Sciences Laboratory PO Box 1500 Edinburgh, South Australia, Australia 5111		
6a. DSTO NUMBER DSTO-TR-1383		6b. AR NUMBER AR 012-547		6c. TYPE OF REPORT Technical Report	
7. DOCUMENT DATE February, 2003					
8. FILE NUMBER E9505/23/162	9. TASK NUMBER NAV 00/107	10. SPONSOR DGNVSY	11. No OF PAGES 36	12. No OF REFS 38	
13. URL OF ELECTRONIC VERSION http://www.dsto.defence.gov.au/corporate/reports/DSTO-TR-1383.pdf			14. RELEASE AUTHORITY Chief, Weapons Systems Division		
15. SECONDARY RELEASE STATEMENT OF THIS DOCUMENT <i>Approved For Public Release</i> OVERSEAS ENQUIRIES OUTSIDE STATED LIMITATIONS SHOULD BE REFERRED THROUGH DOCUMENT EXCHANGE, PO BOX 1500, EDINBURGH, SOUTH AUSTRALIA 5111					
16. DELIBERATE ANNOUNCEMENT No Limitations					
17. CITATION IN OTHER DOCUMENTS No Limitations					
18. DEFTTEST DESCRIPTORS Flow,Mathematical Models,Microstructure,Porosity,Energetic Materials					
19. ABSTRACT A new reactive flow model for heterogeneous energetic materials has been developed based on the physical and chemical parameters of the material as much as possible, rather than solely relying on empirical constants to determine the reaction rates behind the shock wave. Firstly, this report presents an extended viscoplastic pore collapse (hot spot) model based on previous models presented in the literature. Results from this hot spot model are then used to develop a reactive flow model embedded into the multi-material hydrocode, MULTI, using an Induction-Parameter-Model to describe the thermo-mechanical processes of pore collapse in a computationally efficient manner. One and two-dimensional hydrocode results are presented for the energetic material HMX undergoing bare and cased projectile impact. The results show the importance of microstructure in determining the shock ignition and subsequent growth behaviour in energetic materials. Thus, a new capability is described for determining the effects of varying porosity (due to manufacture, aging, damage, etc) on shock sensitivity and can be used to help evaluate the Insensitive Munitions (IM) qualities of weapon systems.					